THESIS FOR THE DEGREE OF DOCTOR OF PHILOSOPHY

Housing Aquaporins in Nanostructured Glass

SIMON ISAKSSON

Department of Chemistry and Chemical Engineering
CHALMERS UNIVERSITY OF TECHNOLOGY
Gothenburg, Sweden 2019

Housing Aquaporins in Nanostructured Glass

SIMON ISAKSSON

ISBN 978-91-7597-851-2

Doktorsavhandlingar vid Chalmers tekniska högskola
Ny serie nr 4532
ISSN: 0346-718X

Department of Chemistry and Chemical Engineering
Chalmers University of Technology
SE-412 96 Gothenburg
Sweden
Telephone + 46 (0)31-772 1000

Cover: Photograph of water in an hourglass, symbolizing water transport through aquaporins stabilized by glass

Chalmers Reproservice
Gothenburg, Sweden 2019

Housing Aquaporins in Nanostructured Glass

SIMON ISAKSSON

Department of Chemistry and Chemical Engineering

Chalmers University of Technology

ABSTRACT

Proteins are a group of biomolecules that perform versatile tasks, which in many cases are essential for life. The magnitude of their importance is perhaps expressed by the word protein itself, coined by the Swedish chemist Jöns Jacob Berzelius in the summer of 1838. It is derived from the Greek word πρωτείος which means 'primary' or 'of the highest importance'. By adding a different ending, Berzelius shaped the word protein which means 'the most important building block in a thin thread'.

The proteins of importance to this PhD thesis are aquaporins, whose primary function in nature is to sustain the osmotic balance across the cell membrane by transporting water. This transportation is highly energy efficient and selective compared to artificial processes, which renders aquaporins interesting from a water purification point of view. Many proteins, including aquaporins, are however not stable in non-native environments, which often results in protein degradation or aggregation upon use in synthetic environments. This is particularly prominent for membrane proteins, which need to be housed in an amphiphilic environment to function properly.

This thesis explores aquaporin stabilization through different kinds of interactions with glass. Human Aquaporin 4 was either intercalated with a mesoporous silica substrate or covered in a thin layer of silica. In both cases, aquaporins were stabilized by a lipid bilayer that mimics its native cell membrane surroundings. This thesis also includes work on the first structural and functional characterization of Climbing Perch Aquaporin 1 and a synthesis method for producing uniform silica nanoparticles with accessible mesopores.

Detailed characterization provided valuable information on different kinds of aquaporin-silica interactions. Aquaporins were, for instance, shown to extend into a porous silica substrate underneath a supported lipid bilayer. Furthermore, aquaporin secondary structure was preserved when stabilized by a silica shell. The findings in this thesis show that silica may be used as a biocompatible stabilization option for aquaporins, potentially paving the way for better aquaporin utilization in applications such as water purification.

Keywords: aquaporin, silica, membrane protein, silicification, formation, interface, water

LIST OF PUBLICATIONS

This thesis is based on work described in the following papers:

I	Mesoporous silica nanoparticles with controllable morphology prepared from oil-in-water emulsions Gustafsson, H.; Isaksson, S.; Altskar, A.; Holmberg, K. *J. Colloid Interface Sci.* **2016,** 467, 253-260.
II	Protein-Containing Lipid Bilayers Intercalated with Size-Matched Mesoporus Silica Thin Films Isaksson, S.; Watkins, E. B.; Browning, K. L.; Lind, T. K.; Cardenas, M.; Hedfalk, K.; Hook, F.; Andersson, M. *Nano Letters* **2017,** 17, (1), 476-485.
III	Formation Mechanism of Silica-Stabilized Aquaporin Proteoliposomes Isaksson, S.; Lotsari, A.; Schmitz, F.; Kjellerup Lind, T.; Barnsley, L.; Prevost, S.; Hedfalk, K.; Lund, R.; Hook, F.; Andersson, M. *Submitted*
IV	Novel structural mechanism of extracellular gating of aquaporin from the fish climbing perch (*Anabas testudineus*) Zeng, J.; Schmitz, F.; Isaksson, S.; Arbab, O.; Andersson, M.; Törnroth-Horsefield, S.; Swaminathan, K.; Hedfalk, K. *Manuscript*

The papers are appended in the end of the thesis.

CONTRIBUTION REPORT

I	Performed all experimental work except for TEM analysis and epoxy embedding.
II	Performed all experimental work, cryo-TEM was co-analysed and NR data was co-modeled. Wrote the manuscript.
III	Performed all experimental work except for protein expression, protein purification, and electron microscopy. Co-modeled the SANS data and wrote the manuscript.
IV	Planned and performed parts of the stopped-flow measurements and DLS measurements. Analyzed the stopped-flow data.

ACKNOWLEDGEMENTS

I will look back on the years spent as a PhD student with much joy. Working on this project in this division has been both enjoyable and exciting for the most part, largely due to the fantastic people involved in the project and in life outside the project. My original idealistic view of the collaborative spirit that catalyzes academic advancements has turned more realistic along the way, but I am glad that this spirit nurtured the collaborations that I was involved in. I want to express as much appreciation as possible to all my colleagues, friends and family that have been there during better and worse times. Your direct and indirect contributions to this thesis are invaluable.

I would like to acknowledge my supervisor Martin Andersson for being the perfect mentor and companion during these years. I could not wish for better guidance in how to develop into an independent researcher or how to conduct high quality research through curiosity and fearlessness. You have been essential to the development of the project and I am thankful for your active participation and continuous enthusiasm along the way.

I am also grateful to my assistant supervisor Fredrik Höök, whose ability to view things from a different perspective has helped me to develop as a critical researcher. Many interesting thoughts have come about during discussions with you and through your active involvement in the project.

I would like to thank the present and former members of the M.A. Research group for being such a cheerful group of people that have provided me with a great working environment. My former office mate Emma, my predecessor Maria Wallin, Chlor, Johan, Anand, Saba, Mats, Gustav, Andy, Astrid, Maria Pihl, and Ali for making work fun, you are all great!

Co-authors, collaborators, and instrument scientists are acknowledged for providing me with the opportunity to learn more about the techniques and research areas that you are experts in. Krister Holmberg and Hanna Gustafsson are acknowledged for giving me the opportunity to learn how to synthesize and characterize silica particles. Kristina Hedfalk and Florian Schmitz are acknowledged for aquaporin expression and purification. Marité Cárdenas and Reidar Lund with their respective groups are acknowledged for providing me with skills in how to perform neutron experiments and model neutron data.

The people at the Divisions of Applied Chemistry and Biological physics are welcoming and fun, which contributes to an awesome working environment. I would like to thank Åsa Östlund and Lars Nordstierna for inviting me to TYK as well as Jonatan and Alex for taking great care of me from the beginning. I would also like to thank Hudson, Mokhtar, and Silver for rewarding collaborations and discussions and my current office mate Szilvia for maintaining the positive atmosphere in the office despite my intense writing.

Sharing knowledge is equally rewarding as obtaining new skills, and I have been fortunate to have the pleasure of supervising Maria, Gustav, and Fredrik in their journey to become Masters of Science. I also applied knowledge transfer in another context, spending six months of the PhD project as a "Playful scientist" in the science center Universeum. Those six months were very exciting and helped me to develop many new skills. I would therefore like to thank the energetic team at Universeum, especially the always positive and enthusiastic Tea. The Swedish Research Council FORMAS is also acknowledged for the flexibility in this matter and for providing the funding to make this PhD project happen.

As a member of the K & BIO PhD student council I have participated in a lot of important discussions. I am sure that the council will continue to passionately care about improving the working conditions of PhD students and support those in need. Thank all of you caring PhD students in the council for all the fun activities and meetings!

Innebandy is a great way to improve the working environment and I would like to thank all of you that have joined me in countless hours of chasing a ball around a court!

Last but not least I would like to thank my family and the friends that have not already been mentioned. You provide me with all sorts of wonderful reasons not to think about work all the time, for which I am grateful. Your interest in the PhD project has at the same time elevated my motivation and helped me to realize the importance of my work. Massive thanks to my family for all the support throughout the years. The appreciation I receive for who I am regardless of what I do for a living provides me with confidence and calmness. The ones that have been affected the most by the production of this thesis still provide me with unconditional appreciation, for which I am forever thankful. This would not have been possible without the energy I receive from you and the sacrifices that you have made, Malin and Lukas.

List of Abbreviations

AQP	Aquaporin
AWC	Artificial water channel
bAQP1	Bovine aquaporin 1
BCP	Block copolymer
BET	Brunauer-Emmet-Teller
BJH	Barrett-Joyner-Halenda
β-NG	*n*-nonyl-β-D-glucoside
β-OG	*n*-octyl-β-D-glucoside
CA	Cardiolipin
CD	Circular dichroism
CHIP28	Channel-forming integral protein of 28 kDa
CM	Contrast matching
CMC	Critical micelle concentration
CNT	Carbon nanotube
cpAQP1aa	Climbing Perch aquaporin 1
CPP	Critical packing parameter
Cryo-TEM	Cryogenic transmission electron microscopy
CTAB	Cetyltrimethylammonium bromide
DLS	Dynamic light scattering
EDX/EDS	Energy-dispersive X-ray spectroscopy
EFTEM	Energy filtered transmission electron microscopy
EISA	Evaporation-induced self-assembly
FRAP	Fluorescence recovery after photobleaching
HAADF	High-angle annular dark-field
hAQP4	Human aquaporin 4
HMM	Hiroshima mesoporous material
IP	Indolocarbazole-pyridine
NPA	Asparagine-proline-alanine amino acid sequence
NR	Neutron reflectivity
P123	Poly(ethylene glycol)$_{20}$-poly(propylene glycol)$_{70}$-poly(ethylene glycol)$_{20}$
PC	Phosphatidylcholine
PCR	Polymerase chain reaction
PCS	Photon correlation spectroscopy
PE	Phosphatidylethanolamine
PG	Phosphatidylglycerol
PLR	Protein-to-lipid ratio
POPC	1-palmitoyl-2-oleoyl-*sn*-glycero-3-phosphocholine
PS	Phosphatidylserine
pSLB	Protein-containing supported lipid bilayer
QCM-D	Quartz crystal microbalance with dissipation monitoring
QELS	Quasi-elastic light scattering
RI	Refractive index
RO	Reverse osmosis
SANS	Small-angle neutron scattering
SAXS	Small-angle X-ray scattering
SDGs	Sustainable Development Goals
SEM	Scanning electron microscopy
SF	Selectivity filter
SiO_2	Silica, Silicon dioxide
SLB	Supported lipid bilayer
SLD	Scattering length density
STEM	Scanning transmission electron microscopy
TEM	Transmission electron microscopy
TEOS	Tetraethyl orthosilicate
TFC	Thin film composite
TIRF	Total internal reflection fluorescence
W/O/W	Water-in-oil-in-water

Contents

In the spirit of Mathias,
whose fight for sustainable solutions ended far too early

1 The big picture

> “Clean water is so basic to human life that water droplets, bubbling brooks and waterfalls are enduring symbols of the life force”

Sushil K. Khetan & Terrence J. Collins[1]

It is fascinating that something as deceivingly simple as water plays such an important role in all of life that it is often used to symbolize life itself. Be it water droplets, bubbling brooks or waterfalls, there is something special about water that is difficult to express in words. Water is also mesmerizing at a global scale, as exemplified by two of the most iconic and widely distributed photographs of all time; “Earthrise” captured by William Anders in 1968 (Fig. 1) and “Blue Marble” captured by the Apollo 17 crew in 1972 (Fig. 2).[2, 3] The blue appearance of Earth is caused by water.

Figure 1: “Earthrise” [Photo credit: NASA]

Figure 2: "Blue Marble" [Photo credit: NASA]

These two photographs have been extensively used by environmental movements, propagating to keep Earth as clean and healthy as it appears from space. Earthlings can, however, easily see past the initial appearance of our planet to realize that things are not as clean and peaceful as these photographs convey. Not even the crispness of the finest medium format Hasselblad cameras could possibly capture the complexity of the world we live in, which is to 71% dressed in reused water.[4]

The importance of *clean* water to humanity is nicely captured in the initial quote from Khetan and Collins.[1] Despite its clean appearance from space, Earth is plagued by unresolved issues; some of which revolve around water. Large-scale water-related issues are nowadays monitored from space, such as ground water levels in California[5] and the massive volume reductions of the Aral Sea and Lake Chad caused by extensive irrigation.[6, 7] Such issues, however, only account for a small fraction of the global water-related issues. Despite the clean appearance of Earth and its oceans from space, there are plenty of problems lurking beneath the surface, many of which are not even perceivable upon ocular inspection from up close. Such issues include water contamination by pharmaceutical residues[1], heavy metals[8], and microplastics[9] along with a range of other pollutants present at elevated levels due to anthropogenic activities such as industrial production and agriculture. Despite awareness of the issue, water pollution is sadly increasing.[10]

The big picture tells us that water pollution is happening at large scale. In an anthropocentric context, polluted water puts 844 million people (11 % of the population on Earth) that do not have access to basic drinking water services[11] at immediate risk of exposure to toxic levels of polluting substances. Indeed, "clean water is so basic to human life" that water pollution may, in extension, be regarded as a threat to humanity. As a consequence, access to clean water is defined as a human right by the United Nations.[12] In a less anthropocentric take on this topic, danger to all living entities is apparent. These issues were acknowledged by the United Nations and included in The 2030 Agenda for Sustainable Development,[13] where one of the paragraphs within goal 6 of the Sustainable development goals (SDGs) reads:

SDG target 6.3

By 2030, improve water quality by reducing pollution, eliminating dumping, and minimizing release of hazardous chemicals and materials, halving the proportion of untreated wastewater and substantially increasing recycling and safe reuse globally.[13]

Many argue that the environmental movement was in part spurred by the photograph Earthrise,[2] which was captured using a camera developed and adapted for space usage by Hasselblad in Gothenburg, Sweden. Gothenburg was also the location where years of research geared towards the development of highly selective and energy-efficient water filtration resulted in the PhD thesis you are currently reading. Which brings us back to Earth and the context of this thesis; the potential use of biomimicry in water treatment to make Earth as clean as it looks in the photographs.

2 Water treatment

In society, water treatment is often encountered as drinking water purification or waste water treatment, commonly representing the beginning and end of human water usage. Both processes usually include several treatment steps in order to reach a desired level of purity, where at least one step includes filtration. Filtration is for instance employed to prevent undesired compounds in drinking water and to limit the extent of pollution exerted upon marine ecosystems by waste water discharge.

Filters used in water treatment can be divided into two main categories: Size exclusion filters and solution-diffusion filters. Size exclusion filters have a certain pore size, and hence prevent substances that are larger than the pores from entering the permeate. A limitation of these filters is that the pore size cannot be tuned to small enough diameters to stop for example sodium and chloride ions to pass, which is needed in drinking water production from sea water, i.e. desalination. Drinking water production from sea water is becoming increasingly popular due to decreasing amounts of available and sufficiently pure fresh water.[14] Solution-diffusion filters are crucial in desalination, which is commonly conducted through reverse osmosis (RO). The selective layer in RO filters usually consists of a thin film composite (TFC) polymer membrane formed in an interfacial polymerization process.[15] Water filtration through TFC membranes is based on a solution-diffusion mechanism in which water is first molecularly dissolving into a polymer matrix at the side of high chemical potential, whereby it diffuses through the polymer down a chemical potential gradient to finally desorb on the side of low chemical potential. To overcome the osmotic pressure involved, pumps are used to drive the filtration process. The rate limiting step is the diffusion through the polymer matrix, which can be improved on the expense of decreased selectivity.[16] Solution-diffusion filters hence suffer from sub-optimal water diffusion rates and therefore need large amounts of energy to purify water.[14]

Energy consumption accounts for about half of the total cost of drinking water production using desalination.[17] The desalination process (membrane or thermal) generally comprises (1) intake, (2) pre-treatment, (3) desalination, (4) post-treatment, and (5) concentrate management, all of which require energy. Pre- and post-treatment consume the largest amount of energy, but they are closely linked to the desalination step. For example, implementing a desalination step that is more resistant to fouling has the potential to significantly decrease the total energy consumption of drinking water production from sea water by lowering the requirements on the pre-treatment step.[4, 18]

2.1 Natural water filtration

Nature possesses methods to filter water on different length scales and to varying levels of purity. A prominent element of the big picture is the water cycle that recycles water through evaporation, condensation and precipitation. This process is nicely illustrated by the presence of clouds in Figures 1 and 2. The water cycle is, however, a thermal process and does therefore not qualify as filtration. An example of large-scale water filtration in nature is the filtration of precipitated water through soil, gravel and rock in the ground that eventually results in the collection of groundwater.

In the other end of the spectrum, nature performs water filtration on the nanometer to Ångström length scale across the cell membrane of all living cells. Cell membranes are based on a lipid bilayer assembly that hosts cell membrane entities such as membrane proteins. Proteins that transverse the cell membrane are called transmembrane or integral proteins and some of these provide gateways across the membrane. These gateways are typically pores that may conduct compound-selective transport of for example calcium ions[19], potassium ions[20], or water[21]. The water-channeling proteins are called aquaporins and they are central to this thesis.

2.1.1 Aquaporins

Aquaporins are a group of transmembrane proteins that were first encountered in erythrocytes by Benga et al. in 1986.[22] In 1988, Denker et al.[23] purified the first aquaporin (initially called CHIP28, short for channel-forming integral protein of 28 kDa), but its biological function remained unclear. Four years later, the same group made the discovery that this protein selectively transports water across the cell membrane,[21] and shortly thereafter renamed it Aquaporin 1. The findings by the group of Peter Agre[21, 23] were eventually rewarded half of the 2003 Nobel prize in Chemistry. Following these initial reports, aquaporins have been discovered in both prokaryotes and eukaryotes at all levels of life.[24] There are 13 human aquaporins, which are divided into three subgroups; water selective (orthodox) aquaporins that solely transport water (AQP0, 1, 2, 4, 5, 6, 8), aquaglyceroporins that (in addition to water) transport small uncharged solutes such as glycerol (AQP3, 7, 9, 10), and superaquaporins (AQP11, 12), whose transport characteristics are to be further elucidated.[25]

The excellent water selectivity of orthodox aquaporins is the result of a channel design that guides the water molecules through the protein in an intricate way. Aquaporins are hourglass-shaped transmembrane proteins with 6 alpha-helices fully spanning the cell membrane and two shorter alpha-helices oriented in such a way that they form a pseudo membrane-spanning helix. The parts of the shorter alpha-helices that face the narrow pore are called NPA-motifs since they consist of the amino acid sequence asparagine-proline-alanine (NPA in short). These motifs equip the aquaporin with an electrostatic barrier that blocks the passage of charged species.[26, 27] The other channel region of extra importance is the selectivity filter (SF), which is located towards the extracellular side. It is defined by an arginine side chain and an aromatic side chain extending into the pore. In the SF of the human aquaporin 4 (hAQP4) that was the aquaporin of choice for the silica stabilization studies, a histidine residue reaches into the channel to restrict the pore diameter to ~1.5 Å.[27] Water molecules are transported through the aquaporin in a single line, while forming transient hydrogen bonds with the amino acid side chains in the pore walls. These hydrogen bonds orient the water molecules and significantly perturb hydrogen bonding between neighboring water molecules, which is an important feature that allows aquaporins to prevent proton transport via a Grotthuss mechanism.[28]

2.2 Biomimicry in water filtration

Mankind has copied large-scale natural water treatment processes for a long time to produce clean water. One of the obvious examples is the utilization of slow sand filters in waterworks.[29] Copying nature is called biomimicry, an expression coined by Schmitt in 1957. Biomimicry means to mimic biology or nature, using biologically inspired designs or making use of entities derived from nature.[30]

Advances in protein engineering and nanotechnology have opened up possibilities of utilizing biomimicry to perform highly selective water treatment. The main driving force to use this kind of approach is the potential to combine high selectivity with high flux, which is not possible using synthetic TFC membranes.[14] The development of filters based on biomimicry has proven problematic due to the limited stability of biological components such as aquaporins outside their native environment.[31] Different approaches have therefore been explored in order to produce biomimetic filters that are stable enough for real-world use.

One approach explored in order to stabilize aquaporins was to deposit aquaporin-containing supported lipid bilayers (SLBs) or proteoliposomes on porous supports.[32-34] The most popular approach to date judged from scientific output is based on aquaporin insertion into amphiphilic block copolymer (BCP) bilayers as pioneered by Stoenescu et al.[35] The same group later showed aquaporin functionality using a polymer-based stabilization approach[36], which has since been developed further for water purification by the same group[37, 38] and others.[39-42] Aquaporins have also been stabilized using other organic molecules such as bolaamphiphiles[43] and in two-step processes where amphiphilic peptides were used for initial aquaporin stabilization followed by subsequent polymeric stabilization.[44, 45] Two-step processes in which

aquaporin-containing proteoliposomes were first deposited on a porous support and subsequently stabilized by polyamide addition were also reported.[46, 47] Membrane designs incorporating aquaporins do, however, so far lack the stability needed for practical use in desalination.[4]

There are also examples of biomimetic approaches omitting the aquaporins. For example, carbon nanotubes (CNTs) were predicted to conduct water at high flux[48] and have since been inserted into lipid bilayers for filtration purposes.[49-51] An all-synthetic approach was also presented, where CNTs were inserted into amphiphilic BCP membranes.[52] Other examples of artificial water channels (AWCs) that mimic aquaporin functionality include zwitterionic channels[53], rigid macrocycle nanotubes[54], imidazole-quartet channels[55], indolocarbazole-pyridine (IP) oligomers[56], and pillar[5]arene channels.[57] Pillar[5]arene channels were included in an all-synthetic design by channel incorporation in a BCP membrane.[57]

Despite the extensive list of approaches mentioned in the previous paragraphs, the commercial potential of nanoscale biomimetic water filtration is little explored. In fact, the only designs that have progressed into commercial products so far are based on aquaporin stabilization by lipid bilayers or BCP membranes. The main reason for the limited commercial success is manufacturing difficulties, in particular related to formation of macroscopic defects in the selective layer.[18] Despite the efforts invested in the development of biomimetic water filters through a variety of creative approaches, this area of research has therefore not yet been able to deliver real-world performance that is on par with its predicted potential.

3 Thesis put into perspective

Perhaps the dark blue picture painted so far was not to your liking? To be honest I am not satisfied with the current situation either. Starting with this chapter, I will therefore try to paint a brighter picture. The canvas of that picture will still be the Earth, but the paint that makes it come to life will be a fresh nuance of blue that has the potential to make the picture appear brighter. The foundation of this paint is a new biomimetic approach called *housing aquaporins in nanostructured glass*. My hope is that an implementation of this approach will result in a brighter future by making biomimetic water filtration realize its full potential.

This is needed because current water treatment solutions are simply not good enough. The demand for clean water is constantly increasing with a growing global population, while water is becoming increasingly polluted. Traditional water treatment technologies are not able to provide humanity with clean drinking water. They are in addition equally insufficient in handling the increasing pollution of water in the environment, which affects all of life. We are hence in need of new solutions, and biomimetic approaches show great promise. Biological systems are, however, typically more fragile than their man-made counterparts, which is why attempts to develop more robust biomimetic membranes with retained filtration potential are currently undertaken. A satisfactory solution is, however, yet to be found.

This thesis presents my approach, which essentially comprises two-step biomimicry. Aquaporins are first incorporated into a lipid bilayer for retained functionality, forming a proteoliposome. The proteoliposome is then either coated with a thin layer of silicon dioxide (silica) or collapsed onto a mesoporous silica substrate to form a protein-containing supported lipid bilayer (pSLB). Silica is the main constituent of sand and it is very abundant in the Earth's crust.[58] Living organisms such as siliceous sponges form hard protrusions, known as spicules, from bio-silica. Aquaporins are key in spicule formation since they transport water that is formed during the condensation of orthosilicic acid into silica away from the spicules, which results in silica hardening.[59] Aquaporins and silica is hence a naturally occurring combination that was used as an inspiration to the work presented in this thesis.

The remaining chapters of this thesis describes the two-step biomimicry approaches used in the process of *housing aquaporins in nanostructured glass*.

4 Aim & Train of thought

The aim of the work presented in this thesis was to evaluate the combined use of lipid bilayers and silica to stabilize aquaporins, with the long-term objective to incorporate aquaporins in applications such as filters for water treatment. Different approaches within the context of *housing aquaporins in nanostructured glass* were explored, which resulted in the development and evaluation of these designs:

- Aquaporins in supported lipid bilayers on mesoporous silica substrates
- Aquaporins in proteoliposomes coated by a thin layer of silica

This thesis describes the stepwise evolution of these designs. Furthermore, the synthesis of mesoporous silica particles and the structural and functional characterization of a fish aquaporin are included in this thesis as components of interest in further developments of the presented stabilization strategies. The publications in this thesis are connected by the train of thought presented below:

Publication I describes the synthesis of mesoporous silica particles, which may potentially be used as pSLB supports. **Publication III** presents another approach utilizing spherical geometry, in which aquaporin-containing proteoliposomes were coated in a thin layer of silica. A combination of publications I and III where the proteoliposome is wrapped around a mesoporous silica particle could potentially be useful in applications requiring additional stabilization. This approach is, however, not pursued in this thesis. **Publication II** introduces the use of a planar stabilization geometry by forming pSLBs on mesoporous silica thin films, where the aquaporins extend both into the pores of the silica and into the bulk on the opposite side of the bilayer. Finally, **Publication IV** describes the structural and functional characterization of climbing perch aquaporin 1 (cpAQP1aa). In contrast to hAQP4 (used in publications II and III), cpAQP1aa allows one of the extracellular loops to fold and block the channel. Stabilization of cpAQP1aa using either of the strategies presented in publications II and III was not conducted, but it is noted that such a design may be of interest in applications where controlling the water flux is of importance.

5 Aquaporin stabilization strategies

Proteins are biological molecules that perform a wide range of specialized tasks in nature. Many proteins also add substantial value when used in man-made processes. Translation of native protein functionality into synthetic settings is, however, difficult. The introduction of proteins into non-native environments often results in protein aggregation or conformational changes, induced by a lack of proper interaction partners for the protein.

Proteins can be divided into four types; soluble, membrane, fibrous, and intrinsically disordered.[60] Membrane proteins are considered particularly difficult to incorporate into synthetic environments since their native environment consists of the complicated mixture of biological molecules that form the cell membrane. A few membrane proteins are, however, used in applications such as biosensors, affinity chromatography, and enzyme reactors.[61]

Aquaporins are ideal components in water filtration since they combine an excellent selectivity for water with high flux. Aquaporin-based water filters are available for purchase, but the field is still struggling with key issues such as aquaporin stability and the prevention of defects in the selective layer.[4, 62] The field of biomimetic water filtration has lately moved away from native-like lipid bilayer-based designs that offer great aquaporin compatibility and into using polymer-based designs. This is because synthetic polymer-based designs offer better filter robustness compared to lipid-based systems. The details of aquaporin-synthetic polymer interactions are not yet fully elucidated and may be the cause of some of the issues mentioned previously. For example, a recent study indicated minor conformational changes occurring in a protein upon insertion into a triblock copolymer membrane.[63]

This thesis focuses on the development of a selective layer consisting of aquaporins and lipids, which are natural components. In addition, stabilization of aquaporin-lipid structures is performed using silica, which is also a natural component. Stabilizing aquaporins with components that are highly compatible in nature should reasonably be beneficial for aquaporin stability. This chapter describes the aquaporins, lipids and silica used in this thesis in more detail and presents the stabilization strategies that were developed during the course of this PhD project.

5.1 Aquaporins in this thesis

A general overview of aquaporins was provided in section 2.1.1. The purpose of this section is to highlight the distinguishing features of the aquaporins that were investigated in this thesis, i.e. hAQP4 and cpAQP1aa. The crystal structure of hAQP4 was solved previously[27] and its biological functions were thoroughly investigated.[64] In contrast, cpAQP1aa appears only once in the literature.[65] The presentation of cpAQP1aa characteristics given here is therefore to some extent based on the findings in publication IV.

5.1.1 Human aquaporin 4

hAQP4 is a 34.8 kDa protein[66] predominantly located in the perivascular end-feet in the brain.[67, 68] It is found as two different splicing isoforms depending on where the splicing mechanism starts. The full-length protein starts from methionine number 1 (hAQP4M1), whereas the other isoform is spliced so that it starts from methionine number 23 (hAQP4M23). This results in a longer N-terminal domain for the M1 splicing variant and it was shown that hAQP4M23 is prone to array-formation as opposed to hAQP4M1 which does not readily form arrays.[68]

hAQP4M23 was used in this thesis and will therefore simply be denoted hAQP4 from now on for simplicity. The use of this isoform favors higher protein-to-lipid ratios (PLRs) due to tighter protein packing through array-formation as compared to the M1 isoform. Higher PLRs should result in higher water permeability rates due to the possibility to incorporate more water channels (pores) in the lipid bilayer. In addition, the ordered orthogonal array formed by hAQP4 could be used as a clue on how to best tailor interfacing materials to match the spatial distribution of proteins in the lipid bilayer.

The choice of hAQP4 for studies aimed at water treatment applications was based on a collection of characteristics that distinguished AQP4 from other aquaporins. First and foremost, it is an orthodox aquaporin and thereby only transports water and no other small solutes such as glycerol.[25] Secondly, it outperforms the other aquaporins in terms of water permeability rates.[69] In addition, hAQP4 functionality is not inhibited by mercury due to a lack of cysteines in the walls of the channel.[27]

5.1.2 Climbing perch aquaporin 1

Climbing perch (*Anabas testudineus*) is an air-breathing fish that tolerates very versatile living conditions. It can be found in canals, ponds, lakes, swamps, and estuaries in tropical Asia. Some examples of adaptability are the ability to acclimate from freshwater to seawater and that it can travel several hundred meters per trip across land to find water, provided that the ambient air is humid enough.[70]

One explanation to the extreme adaptability involves the aquaporin cpAQP1aa. Despite being a homologue of the human AQP1 that does not transport ammonia it

has been suggested to facilitate both water and ammonia transport across the cell membrane. It is predominantly expressed in the gills and skin of the climbing perch, suggesting that it plays an important role in acclimation to changes in the environment.[65]

The explanation as to why cpAQP1aa could be of great importance to climbing perch adaptability might be related to its structure, which is shown in Figure 3A. cpAQP1aa proteins assemble in tetramers where each protein comprises six membrane-spanning α-helices and a seventh pseudo-transmembrane α-helix that lines the pore. There is also a fifth pore formed in between the four proteins in the tetramer. All of these structural features are shared with other aquaporins. The explanation to cpAQP1aa involvement in climbing perch adaptability might instead be a regulation mechanism. Structural data shows that a leucin in one of the extracellular loops of the aquaporin forms a hydrophobic block inside the pore, which is made possible by a novel fold of extracellular loop C (Fig. 3B). This fold has not been observed in other aquaporins and this regulation mechanism could be a key component in climbing perch adaptability.

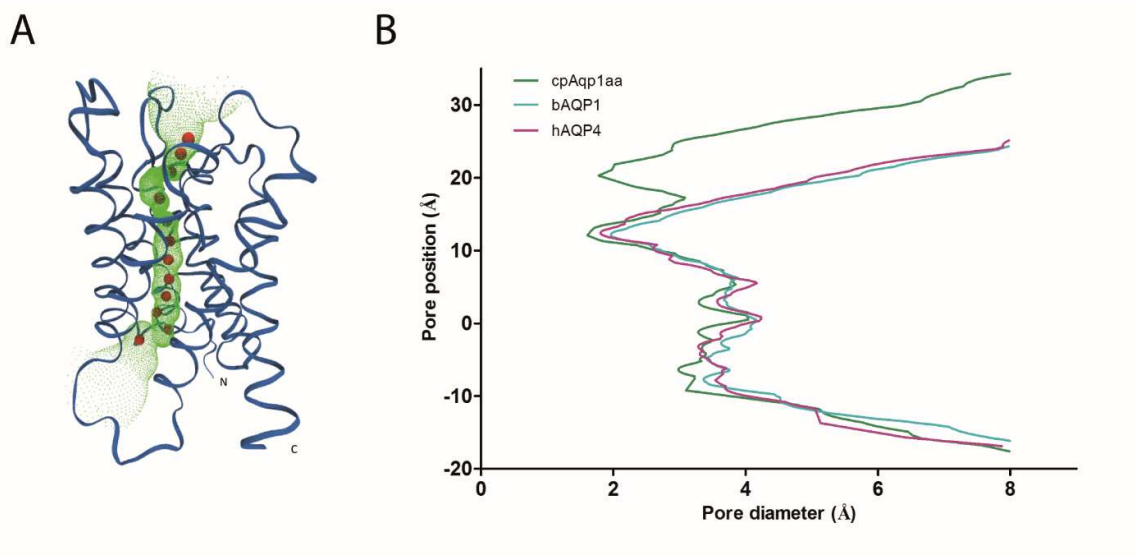

Figure 3. (A) Tunnel representation of cpAQP1aa. Water molecules are shown as red spheres. Green spheres surrounding the water molecules indicate the inner surface of the water conducting pore. (B) Plot of the channel diameter profiles of cpAQP1aa (green), bovine AQP1 (bAQP1, cyan), and hAQP4 (purple). The narrow segment located 20 Å into the pore in cpAQP1aa is a result of extracellular loop C folding into the pore. Figures adapted from Jiao Zeng, PhD thesis, National University of Singapore.

5.1.3 Aquaporin production and purification

A first step to studying aquaporins is to isolate them from their native surroundings that contain other proteins. hAQP4 and cpAQP1aa were recombinantly overexpressed in *Pichia pastoris* yeast cells, followed by cell membrane breakage and protein purification. The genes coding for hAQP4 and cpAQP1aa were amplified through polymerase chain reaction (PCR) and cloned into the *P. pastoris* vectors pPICZB and pPICZA, along with sequences coding for C-terminal hexa-histidine and octa-histidine tags, respectively. The gene coding for cpAQP1aa was also cloned into the pPICZA vector without the additional His-tag. Zeocin screening was performed to select for *P. pastoris* cells that contained genes which coded for the desired aquaporins. For hAQP4, constructs from the selected colonies were linearized and transformed into wild-type *P. pastoris* using the lithium chloride method. The cells were resuspended in LiCl and subjected to heat shock in order for the cell membrane to become permeable to DNA, whereby the linearized DNA was internalized. For cpAQP1aa, viable colonies were tested in small-scale aquaporin production and selected on highest yield. Transformed or selected cells were grown in a bioreactor where aquaporin overexpression was induced by using methanol as the carbon source. The cells were then subjected to breakage, followed by centrifugation to separate cell debris from the crude membrane. The crude membrane was then washed, centrifuged, and solubilized. Solubilized components were collected through centrifugation and from this material, aquaporins were singled out in a Ni-NTA column through selective interactions between nickel ions and histidines. Purified hAQP4 and cpAQP1aa were stabilized in *n*-octyl-β-D-glucoside (β-OG) and *n*-nonyl-β-D-glucoside (β-NG), respectively.

5.2 LIPID BILAYERS

Polar lipids are the main and shape-defining components of membranes present in prokaryotes as well as eukaryotes. They are amphipathic molecules that consist of both hydrophilic and hydrophobic parts. Polar lipids are commonly pictured as molecules having a head and one or more tails, where the head is hydrophilic and the tail is hydrophobic. There are several classes of polar lipids according to structure.[4] The major class in eukaryotic organisms is glycerophospholipids, possessing a glycerol backbone covalently attached to two fatty acid chains and any of a phosphatidylcholine (PC), phosphatidylethanolamine (PE), phosphatidylserine (PS), phosphatidylinositol, or phosphatidic acid head group. From these, more than half of the polar lipids present in eukaryotes are PC.[71] PC is also the most abundant class of lipid in mammalian membranes.[72]

The amphipathic character of lipids results in interesting behavior, such as self-assembly into ordered structures in solution or at interfaces. Lipid concentration and solvent properties are two of the factors that govern the self-assembly process. Due to their cylindrical shape and relatively high critical packing parameter (CPP), lipids arrange into bilayers at lipid concentrations above the critical micelle concentration (CMC). In bilayers, hydrophobic tails are oriented towards the center of the bilayer whereas hydrophilic heads are oriented outwards as illustrated in Figure 4. Lipids can arrange into bilayer structures adopting for example spherical shapes, forming liposomes such as those used in this thesis.

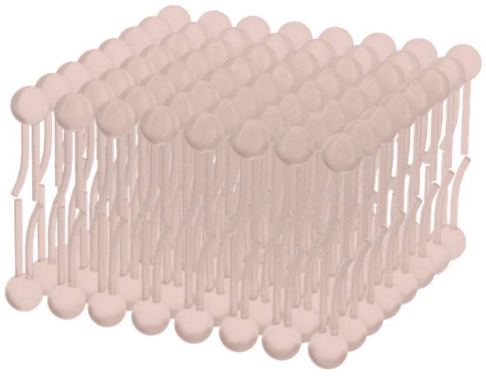

Figure 4: Illustration showing a small segment of a lipid bilayer. Lipids (brown) are illustrated with hydrophilic head groups (spheres) connected to hydrophobic fatty acids (cylinders).

5.2.1 POPC lipids

One of the most well-studied lipids is 1-palmitoyl-2-oleoyl-*sn*-glycero-3-phosphocholine (POPC). It belongs to the PC class of lipids and consists of a hydrophobic diacylglycerol backbone carrying a phosphate group, which is esterified to a choline to form the hydrophilic head group.[71] The isoelectric point of the phosphate group is low, and it is therefore deprotonated and negatively charged at neutral pH. Since the choline group carries a positive charge, the overall net charge at neutral pH is zero. POPC belongs to the group of zwitterionic phospholipids due to the presence of these two opposing charges. The hydrophobic part of POPC consists of two acyl chains, one of 16 carbons that is saturated (16:0) and one of 18 carbons that is mono-unsaturated (18:1). This combination of head group and dual acyl chains (one that is kinked due to mono-unsaturation) results in a CPP in the range 0.5-1 and almost cylindrical lipid geometry that typically packs into bilayers in aqueous solution when the concentration is above the CMC.[71]

5.2.2 *E. coli* polar lipid extract

E. coli polar lipid extract is commonly used for membrane protein reconstitution purposes.[73] The lipid extract used in this thesis was purchased from Avanti Polar Lipids Inc. and had a lipid composition of 67 wt% PE, 23.2 wt% phosphatidylglycerol (PG), and 9.8 wt% *E. coli* cardiolipin (CA).[74] Since it is derived from *E. coli*, it resembles the lipid environment of Gram-negative transmembrane proteins. It has, however, also been used for reconstituting transmembrane proteins of other origins, such as fish aquaporins.

5.2.3 Lipid bilayers as aquaporin hosts

Membrane proteins are typically sensitive to changes in their surrounding environment, which in a native setting consists of the cell membrane. The cell membrane is based on a lipid bilayer and many membrane proteins have been shown to rely on direct protein-lipid interactions[75, 76] and bilayer fluidity[77, 78] to function properly. Direct protein-lipid interactions are sometimes so intimate that tightly bound lipids (annular lipids) can be seen in connection to the protein in detergent stabilized protein solutions used for crystallography. Aquaporins do typically not contain annular lipids that are closely interacting with each protein, but it was shown that a few lipids are present in between the tetramers in orthogonally ordered aquaporin 0.[79] Changes in bilayer composition also altered water permeability rates of AQP4, which implies that aquaporin performance depends on the lipid composition of the bilayer.[80]

Lipid bilayers are commonly used as cell membrane mimics, which was also the case for this thesis. Aquaporin-containing proteoliposomes were prepared as described in section 5.2.3.1. Cryogenic transmission electron microscopy (cryo-TEM) was used to study the size and shape of hAQP4-containing proteoliposomes since aqueous solutions are not compatible with the ultra-high vacuum conditions of conventional transmission electron microscopy (TEM). The micrographs depicting liposomes (Fig. 5A) and proteoliposomes (Fig. 5B) showed clear and interesting differences. The first observation was that bilayer thicknesses among liposomes were more uniform than bilayer thicknesses among proteoliposomes. An assessment of the bilayer thicknesses of 30 liposomes and 30 proteoliposomes from cryo-TEM micrographs showed that there were differences in bilayer thickness between liposomes (Fig. 5C) and proteoliposomes (Fig. 5D). Interestingly, all liposomes in the liposome sample formed a single bilayer thickness population centered around 5 nm whereas the proteoliposome sample consisted of two populations centered around 5 and 7 nm, respectively. This observation was attributed to preferential protein insertion in the reconstitution process, favoring some liposomes over others. In addition, species of the 7 nm population of proteoliposomes were never observed closer than 2 nm from another liposome or proteoliposome. This observation also indicated that both liposomes and proteoliposomes were present in the proteoliposome sample since extracellular domains of hAQP4 would protrude from the bilayer and provide a sterically hindering barrier in between the proteoliposome and its neighbor.

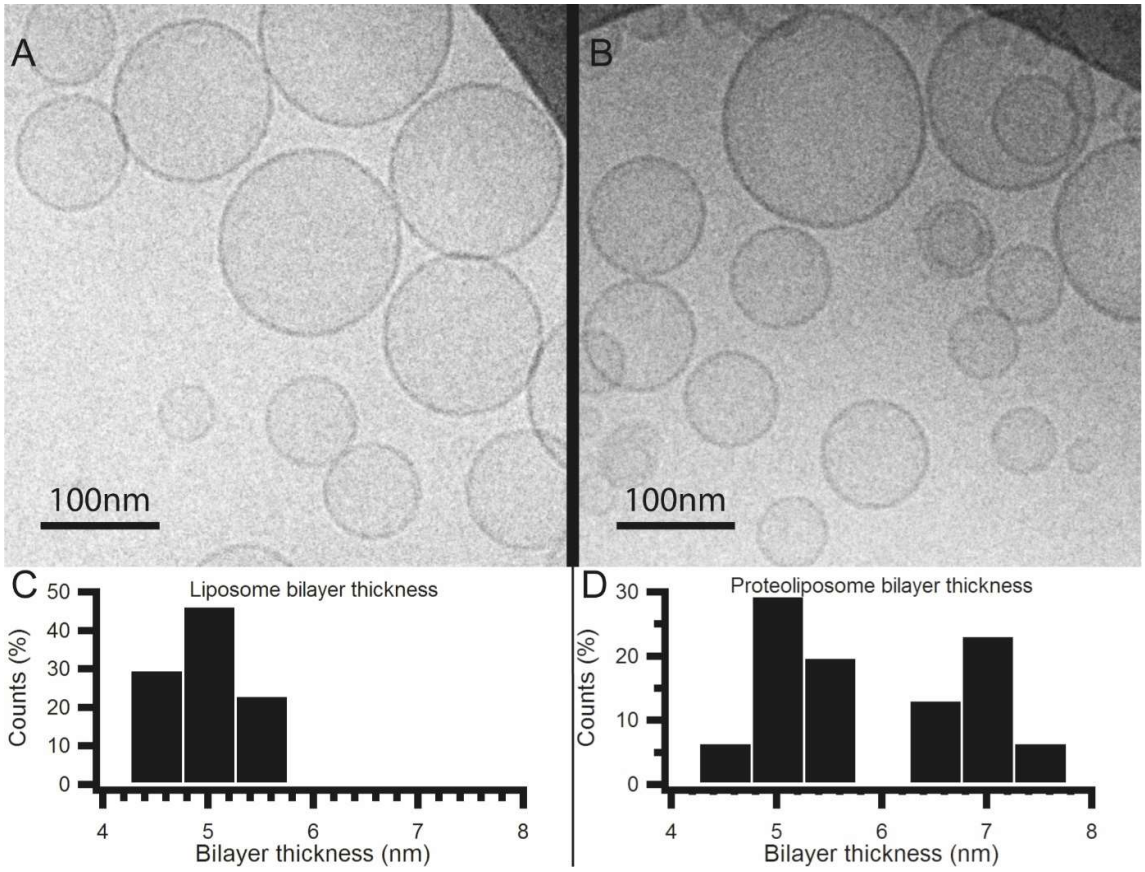

Figure 5. (A) Cryo-TEM micrograph of a POPC liposome sample. (B) Cryo-TEM micrograph of an hAQP4-containing POPC proteoliposome sample. (C) Bilayer thickness distribution of 30 liposomes as determined from POPC liposome samples, showing one population centered at 5 nm. (D) Bilayer thickness distribution of 30 proteoliposomes as determined from hAQP4-containing POPC proteoliposome samples, showing two populations centered at 5 and 7 nm, respectively.

The water transport rate of proteoliposomes was 3 times higher than their corresponding liposomes for both kinds of aquaporins as assessed by stopped-flow light scattering (Fig. 6A). This was in accordance with previously reported observations,[81] and suggests that the proteins are functional.

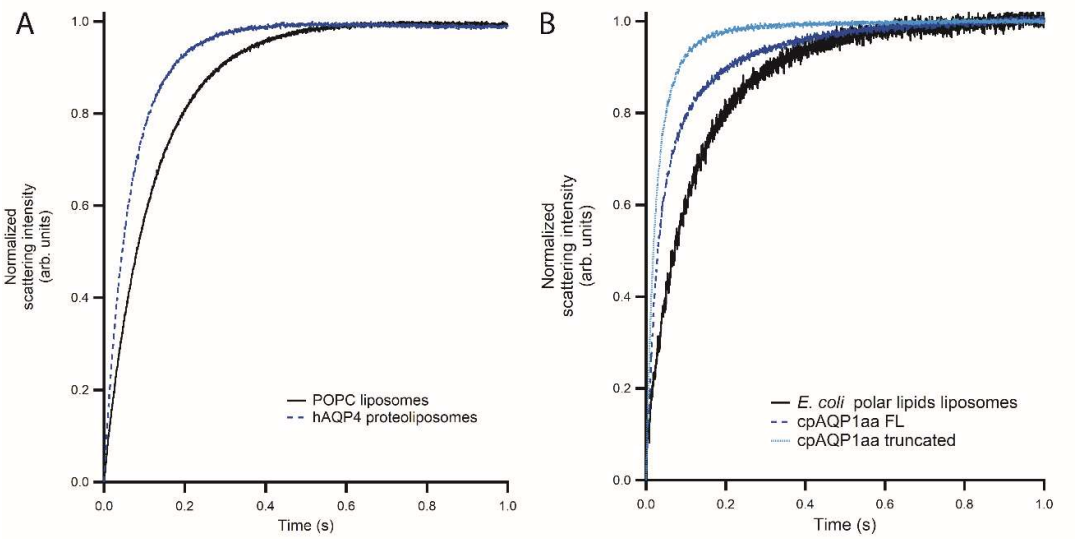

Figure 6: Aquaporin functionality assessments using stopped-flow light scattering. (A) hAQP4-containing POPC proteoliposomes (dashed, blue) compared to POPC liposomes (solid, black). (B) Full-length cpAQP1-containing *E. coli* polar lipid proteoliposomes (dashed, blue) compared to truncated cpAQP1-containing *E. coli* polar lipid proteoliposomes (dotted, light blue) and *E. coli* polar lipid liposomes (solid, black).

5.2.3.1 Preparation of aquaporin-containing proteoliposomes

Proteoliposomes were formed by insertion of purified hAQP4 and purified cpAQP1aa into liposomes made from POPC and *E. coli* polar lipids, respectively. For hAQP4 insertion, POPC was first dissolved in chloroform upon delivery and subjected to rotary evaporation to form a lipid film. The lipid film was resuspended in Tris buffer to yield multilamellar POPC liposomes, which were formed through the process of molecular self-assembly. For cpAQP1aa insertion, *E. coli* polar lipid extract was directly homogenized in Tris buffer to form multilamellar liposomes. Both aquaporins were incorporated into liposomes through a reconstitution process. Liposomes were first mixed with extra Tris buffer constituents to retain the initial concentrations of buffer components upon reconstitution. The liposomes were then partly solubilized in β-OG detergent. Detergent-stabilized aquaporins were added to the partly solubilized liposomes, followed by the subsequent addition of Biobeads SM-2 adsorbent onto which β-OG adsorbed. Detergent adsorption onto biobeads resulted in weakened aquaporin and liposome solubilization, which in turn resulted in spontaneous insertion of aquaporins into liposomal bilayers. This process was driven by the "hydrophobic effect", which aims at minimizing the exposure of hydrophobic transmembrane domains to the aqueous solution. Biobeads were removed by decantation upon detergent withdrawal and the proteoliposomes were subject to spin column filter centrifugation to produce smaller, less polydisperse, and unilamellar proteoliposomes.

5.2.3.2 Characterization of aquaporin-containing proteoliposomes

Characterization of proteoliposomes was performed using electron microscopy and light scattering with the purpose to determine the size and geometry of the proteoliposomes as well as aquaporin functionality.

5.2.3.2.1 Cryogenic transmission electron microscopy

Cryo-TEM was used to study liposomes and hAQP4-containing proteoliposomes because the ultra-high vacuum conditions used in conventional TEM (described in section 5.3.1.5.2) are not compatible with aqueous solutions. In cryo-TEM, the sample is rapidly frozen and embedded in amorphous ice in order to retain its structure. Rapid plunge-freezing of the sample is critical in order to prevent formation of ice crystals that can disrupt the sample structures. Liposome and hAQP4-containing proteoliposome solutions were applied to cupper TEM grids and subject to blotting from the backside of the grid to form a thin layer of sample. The grids were then plunged into liquid ethane (–180 °C) and transferred to a sample stage which was cooled by liquid nitrogen throughout the analysis.

Cryo-TEM analysis was performed using a Philips CM120 cryo-TEM operated at 120 kV acceleration voltage.

5.2.3.2.2 Dynamic light scattering

Dynamic light scattering (DLS), also known as photon correlation spectroscopy (PCS) or quasi-elastic light scattering (QELS), was used to assess the size distributions of POPC liposomes, *E.coli* polar lipid liposomes, hAQP4-containing proteoliposomes, and cpAQP1aa-containing proteoliposomes. In DLS, the sample is irradiated by monochromatic light, which is either absorbed or scattered by the sample. Scattered light is monitored at a certain scattering angle in relation to the incoming light.[82] In dispersed particle systems such as proteoliposomes in buffer, the main contribution to the scattering signal is caused by differences in refractive indices between the proteoliposomes and the surrounding buffer. Time-resolved light scattering measurements are employed to probe the movement of the scattering entities due to diffusion. Relaxation times can be determined from the diffusion characteristics of a sample, which in turn can be used to determine the size of the scattering entities.

A Malvern Zetasizer Nano ZS that operated at a fixed detection angle of 173° was used for the DLS measurements presented in this thesis.

5.2.3.2.3 Stopped-flow light scattering

Stopped-flow light scattering was used to assess the water flux across the bilayers of POPC liposomes, *E. coli* polar lipid liposomes, hAQP4-containing proteoliposomes, and cpAQP1aa proteoliposomes. In stopped-flow light scattering, sub-second kinetics are monitored following an initial rapid mixing of reactants. Upon the initial mixing, the flow is stopped and the transition from the initial state to the final state is monitored using light scattering.

In order to assess the water flux, liposome and proteoliposome samples were mixed with a hyperosmolar solution containing sucrose. The rapid introduction of sucrose to the bulk solution upon mixing resulted in an osmotic gradient across the lipid bilayer. The osmotic gradient induced water flux in the direction of higher osmolarity, i.e. out of the proteoliposomes, in order to dilute the sucrose and thereby balance the concentration of osmolytes across the bilayer. Rapid proteoliposome shrinkage was detected as a change in scattered light as a function of time, which can be fitted to an exponential function on the form

$$I = A_1 \mathrm{e}^{-k_1(t-t_0)} + A_2 \mathrm{e}^{-k_2(t-t_0)} + A_3 \quad (1)$$

where I is the measured intensity, A_1, A_2, and A_3 are coefficients, k_1 and k_2 are rate constants, t is the time, and t_0 is the starting time. The rate constants can then be used to calculate the osmotic water permeability P_f from

$$P_\mathrm{f} = \frac{k}{(S/V_0) \cdot V_\mathrm{w} \cdot c_\mathrm{out}} \quad (2)$$

where S/V_0 is the ratio of external surface area to internal volume, V_w is the partial molar volume of water, and c_out is the external osmolality.[83] S/V_0 was calculated based on the average sizes obtained from DLS measurements.

The stopped-flow light scattering equipment used in this thesis was an SFM 2000 (BioLogic Science Instruments) operated at a fixed 90° detection angle.

5.3 SILICA

Silica (SiO_2) is a very abundant material in the Earth's crust and commonly encountered in everyday life in the shape of sand and as the main constituent in glass.[58] It is widely used in industrial applications in the form of colloidal silica particles, which have traditionally been produced using the established Stöber process.[84] In this process, silica is formed from silicon alkoxides which hydrolyze in the presence of water as

$$\equiv Si - OR + H_2O \leftrightarrow \equiv Si - OH + ROH \quad (3)$$

where the three stacked horizontal lines depict covalent bonds between silicon and the additional alkoxide groups of the silicon alkoxide. Hydrolysis results in the formation of silanol groups (Si-OH), that participate in condensation polymerization reactions as

$$\equiv Si - OR + HO - Si \equiv \leftrightarrow \equiv Si - O - Si \equiv \ + ROH \quad (4)$$

$$\equiv Si - OH + HO - Si \equiv \leftrightarrow \equiv Si - O - Si \equiv \ + H_2O \quad (5)$$

The formed ≡Si–O–Si≡ linkages are called siloxane bridges and form the backbone of silica. In addition to siloxane bridges there are silanol groups present both inside and on the surface of silica. These are more reactive than the siloxane bridges and can therefore be used for functionalization purposes.

5.3.1 Mesoporous silica

Mesoporous silica particles, by definition having pore diameters of 2-50 nm,[85, 86] were first presented by researchers at Mobil corporation in 1992 using surfactants as pore templates.[87] In 1998, Zhao *et al.* produced mesoporous particles with larger pores using block copolymers as templating agents.[88] The common denominator of the surfactants and BCPs used in these groundbreaking studies is that both are amphipathic. They do therefore self-assemble into well-defined structures when dispersed in solution at concentrations above the CMC. This self-assembly results in long-range ordered liquid crystalline phases that can arrange into for example lamellar, cubic or hexagonal structures. These liquid crystalline structures can be used as pore templates in the formation of inorganic material such as silica, which was done in publication II in this thesis. Similar use of amphipathic molecules in templating was shown in publication I, where surfactants stabilized a water-in-oil-in-water (W/O/W) emulsion in which the dispersed oil phase templated the pores of silica particles. In these processes, the arrangement of silica precursor is dictated by

the arrangement of the templates. The silica network is then formed by silica precursor hydrolysis followed by condensation as described in equations 3-5.

Silica precursor hydrolysis followed by condensation around a template can also be used to form mesoporous silica thin films using the convenient evaporation-induced self-assembly (EISA) process introduced by Brinker and coworkers in 1999.[89] In this process, silica precursor and templating molecules are first dispersed in an excess of volatile solvent. The volatile solvent evaporates quickly upon deposition onto a substrate by for example spin-coating or dip-coating, resulting in rapid formation of ordered liquid crystalline structures in the non-volatile solvent remaining on the substrate. The ordered phase can be tuned by altering the ratios between the components according to phase diagrams. Condensation takes place upon solvent evaporation to form a thin film of mesoporous silica on the substrate.[89] The silica precursor used in this thesis was the silicon alkoxide tetraethyl orthosilicate (TEOS).

5.3.1.1 Mesoporous silica particles

Particles were synthesized using the surfactants cetyltrimethylammonium bromide (CTAB), 12-6-12, 12-2-12, and Ethylan 1008 as emulsion stabilizers (indirect pore templating agents). CTAB-templated particles (named MPS-1) were deemed most promising for protein stabilization and are therefore presented here. Details on the other synthesized mesoporous silica particles are found in publication I in this thesis.[90] TEM micrographs depicted the presence of elongated pores in MPS-1 (Fig. 7a).

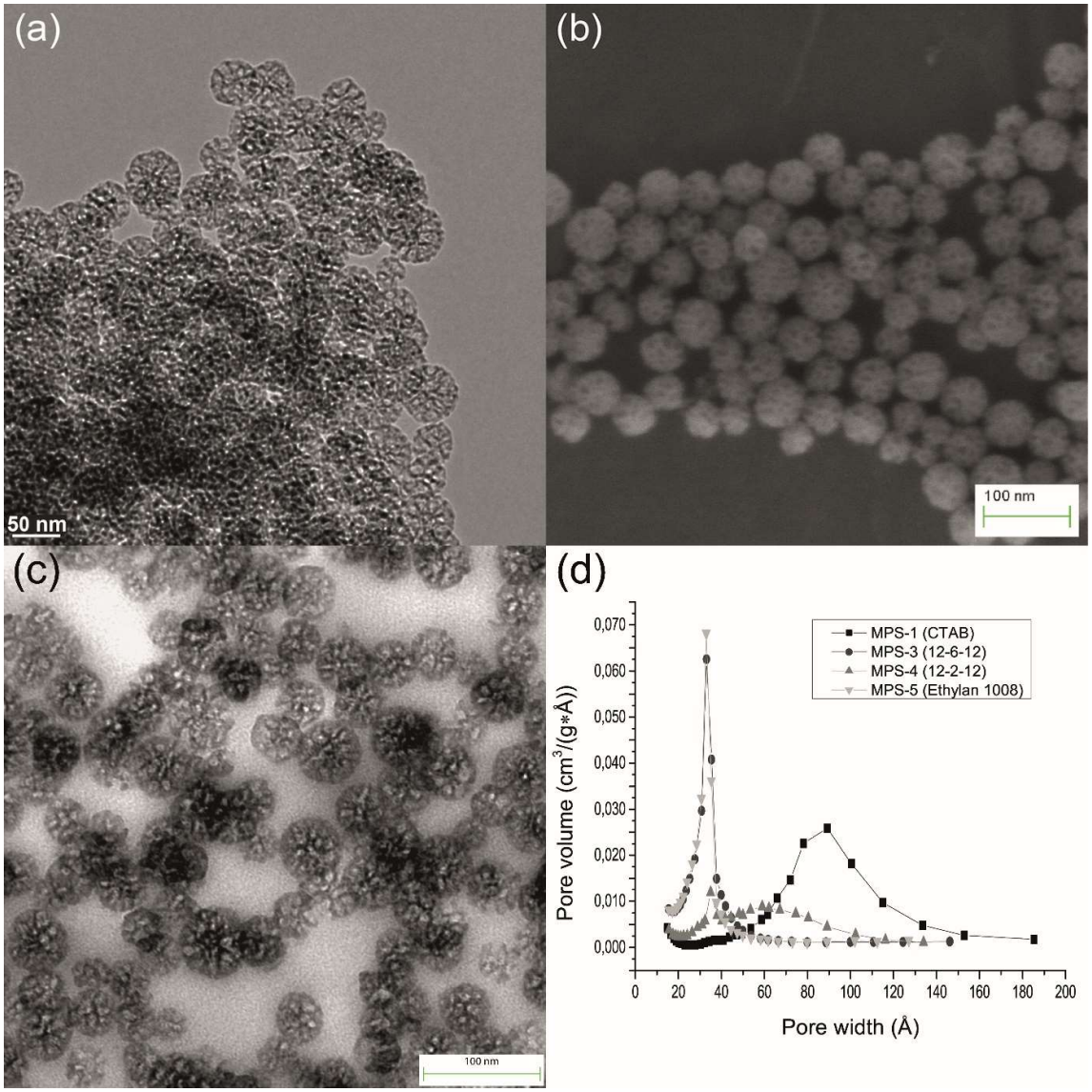

Figure 7. MPS-1 characterization using (a) TEM, (b) SEM, and (c) TEM on epoxy-embedded particles sliced into thin slices. (d) Comparison of pore sizes in the mesoporous silica particles synthesized in this thesis.

Scanning electron microscopy (SEM) micrographs also showed elongated pores that were readily accessible on the surface of MPS-1 particles (Fig. 7b). In comparison, pores in particles synthesized using 12-6-12 and Ethylan 1008 as indirect pore templating agents were hardly distinguishable in SEM and TEM (data shown in publication I). The mean particle diameter of MPS-1 was 53 nm according to TEM and SEM and all of the synthesized samples were similarly polydisperse.

As SEM mainly provided data on the structure of the particle surface and TEM provided data on the particle as a whole, MPS-1 particles were embedded in epoxy and cut into thin (~60 nm) slices. In order to specifically assess the internal pore structure. These slices were studied using TEM (Fig. 7c) and it was concluded that the particle interior showed great similarity to intact MPS-1 particles. This observation strengthened the conclusion that these particles obtained their pore morphology from certain characteristics of the W/O/W emulsion, which was proposed to give rise to the pore structure.

Pore widths were investigated in more detail using N_2 physisorption. The adsorption–desorption isotherms showed Type IV behavior for all of the particles, which is typical for mesoporous materials.[91] Figure 7d shows a comparison of the pore width distributions obtained for the four particles. Particle pore width is of interest in aquaporin stabilization since aquaporins utilize the space underneath the lipid bilayer provided by the pores. The pore width distributions obtained from N_2 physisorption showed that MPS-1 possessed the widest pores among them (~6-14 nm), which should be an advantage over particles with narrower pores in aquaporin stabilization.

5.3.1.2 Preparation of mesoporous silica particles

Mesoporous silica particles with pore widths of interest for protein stabilization purposes were formed and characterized. Hiroshima mesoporous material (HMM) particles introduced by Nandiyanto *et al.* in 2009,[92] were used as inspiration due to their promising characteristics for this purpose. The original particle synthesis protocol turned out to be more complex than necessary and to simplify the synthesis process, the polymer, the polymerization initiator and the inert atmosphere were removed from the synthesis procedure. In addition, the proposed catalyst L-lysine was substituted for ethanolamine in 3 out of the 4 synthesis procedures. Particle sizes and pore morphologies were altered using 3 different surfactants as templating agents, in addition to CTAB that was used in the original synthesis. Particles synthesized using CTAB were denoted MPS-1, whereas particles synthesized using 12-6-12, 12-2-12, and Ethylan 1008 were denoted MPS-3, MPS-4, and MPS-5, respectively. The formation of a water-in-oil-in-water (W/O/W) double emulsion was conducted by vigorous mixing of surfactant, de-ionized water, n-octane and L-lysine/ethanolamine at 70 °C. TEOS was added to the emulsion, entering the oil phase due to the alkoxide hydrophobicity. TEOS hydrolysis was initiated at oil–water interfaces, followed by silica condensation. The reaction proceeded for 20 h, after which the reaction mixture was decanted into a separation funnel. The water phase was collected and freeze dried in order to retrieve the particles, which were then thermally treated to remove organic components.

5.3.1.3 Mesoporous silica thin films

Structural and morphological characterizations of mesoporous silica thin films were conducted using TEM, SEM and small-angle X-ray scattering (SAXS) (Figure 8). The pore arrangement in the mesoporous film was investigated using TEM (Figure 8A) and SAXS (Figure 8B). The q-ratios between the peaks in the SAXS diffractogram revealed that the pores were predominantly hexagonally ordered, which was confirmed by TEM. The pore diameter was uniform at 6 nm, as shown by TEM and SEM (Figure 8C). SEM also revealed that the porous network was accessible from the surface of the film, which meant that the hexagonal phase was oriented with the long axis perpendicular to the substrate. SEM was further employed on the film cross-section to assess the thickness of the mesoporous silica thin film, which was ~300 nm (Figure 8D).

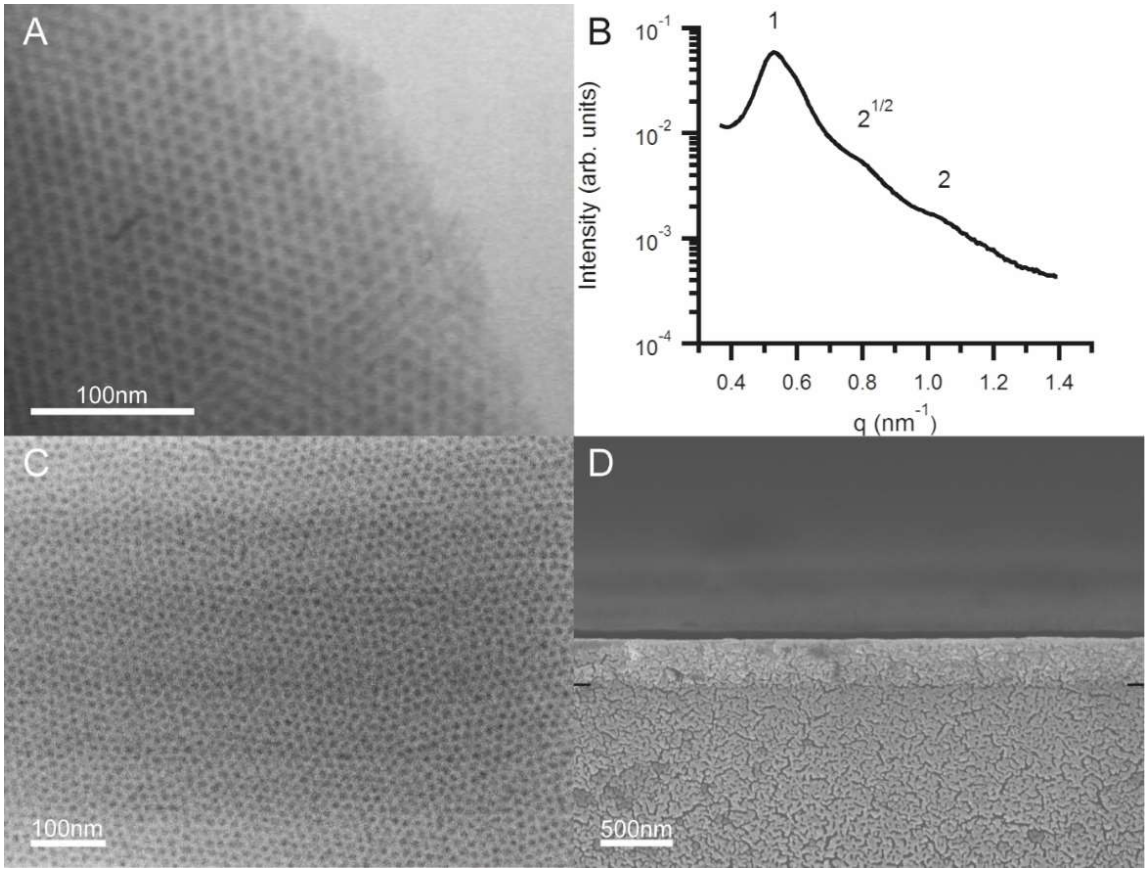

Figure 8. (A) TEM micrograph showing hexagonal ordering of the porous network in the mesoporous silica substrate. The pores are uniform with a diameter of 6 nm. (B) SAXS data providing evidence of long-range hexagonal pore ordering in the mesoporous silica thin film. The numbers above the Bragg peaks denote the relative q-ratios between the peaks. (C) Top view of the mesoporous silica surface captured by SEM. Pores with pore diameters of 6 nm are accessible from the surface. (D) Cross section of mesoporous silica thin film deposited on a glass slide and assessed using SEM (silica–glass interface is depicted by black lines). The mesoporous thin film is ~300 nm thick.

5.3.1.4 Preparation of mesoporous silica thin films

Mesoporous silica thin films were formed using the nonionic block copolymer poly(ethylene glycol)$_{20}$-poly(propylene glycol)$_{70}$-poly(ethylene glycol)$_{20}$ (Pluronic P123) as pore template. In the work described in this thesis, the centrally positioned hydrophobic poly(propylene glycol) chain folds to orient the hydrophilic poly(ethylene glycol) chains in the same direction, which makes it amphipathic.[86] The silicon alkoxide TEOS was used as the silica precursor. Mesoporous silica thin films were prepared on glass substrates, quartz crystal microbalance with dissipation monitoring (QCM-D) crystals, titanium discs, and silicon crystals. TEOS hydrolysis was initiated by mixing TEOS, EtOH and HCl in pH 2. P123 was meanwhile dissolved in EtOH and then mixed with the pre-hydrolyzed TEOS solution. The solution was deposited onto substrates using spin-coating. Rapid evaporation of EtOH during spin coating induced liquid crystalline phase formation in the remaining aqueous phase containing P123. Pre-hydrolyzed TEOS continued to hydrolyze in the presence of water, catalyzed by the low pH. The resulting silanol species condensed and polymerized into silica, which formed around the P123 template. Mesoporous silica was finally obtained following ageing in 20 °C and subsequent heat treatment in 400 °C, during which the organic P123 was burnt off to leave pores within the amorphous silica film.

5.3.1.5 Mesoporous silica characterization

Characterization of mesoporous silica particles and thin films was performed using electron microscopy, X-ray scattering, and N_2 physisorption in order to evaluate the structure and morphology of the materials. The pores in the materials were of extra interest due to the underlying purpose of utilizing these materials in protein stabilization.

5.3.1.5.1 Scanning electron microscopy

SEM analysis is performed in an ultra-high vacuum environment. The sample is scanned by an electron beam, which results in the emission of secondary and back-scattered electrons from the sample surface. In this work, the secondary electrons were collected by a detector to provide information on the topography of the sample surface. Recesses (pores) gave rise to dark areas whereas edges (pore walls) gave rise to brighter features.

The acceleration voltage applied to the electron beam can be adjusted to adapt the analysis according to the requirements of investigation. Silica is a bad conductor, which results in accumulation of electrons from the electron beam in the sample. This results in the introduction of charge effects, which are undesired and can be reduced by lowering the acceleration voltage. Lowering the acceleration voltage decreases the penetration depth of the primary electrons from the beam and hence the detection depth.

In this thesis, SEM analysis on mesoporous silica samples was conducted in the range of 2-5 kV using a LEO Ultra 55 FEG SEM.

5.3.1.5.2 Transmission electron microscopy

Like SEM, TEM analysis is based on the use of an electron beam in ultra-high vacuum. Higher acceleration voltages are used compared to SEM and thin specimens are prepared to allow electrons to be transmitted through the sample. Electrons are scattered on their way through the sample and the scattering magnitude is dependent on the density and thickness of the material. Scattering is monitored by focusing the transmitted electrons onto a fluorescent screen. Dense atoms hinder the passage of electrons, resulting in a dark projection provided that the sample is in the focal plane.

In this thesis, TEM analysis of mesoporous silica films and particles was performed using a JEOL JEM-1200 EX II operated at 120 kV and a FEI Tecnai T20 operated at 200 kV. Thin particle slices embedded in epoxy were analyzed using a LEO 706E operated at 80 kV, whereas silicified liposomes and proteoliposomes were analyzed using a FEI Titan 80-300 operated at either 80 or 300 kV.

5.3.1.5.3 Small-angle X-ray scattering

SAXS was used to study long-range pore ordering in mesoporous silica. X-rays have wavelengths on the order of lattice planes in crystalline materials (hard X-rays; ~0.10-0.15 nm)[93] and are suitable for studying mesoporous materials with repetitive long-range ordered porosity. The sample is exposed to a high intensity X-ray beam and the incoming X-rays scatter upon interaction with the electrons in the material. Photons that are elastically scattered at low angles in relation to the primary X-rays contain information on sample structure. The intensity of the scattered radiation is plotted as a function of the scattering angle 2θ or the momentum transfer q, related as

$$q = \frac{4\pi \sin(\theta)}{\lambda} \qquad (6)$$

where λ is the X-ray wavelength. SAXS studies of long-range ordered materials result in diffractogram Bragg peaks due to constructive interference of scattered radiation. The relation between Bragg peaks was used to assess the long-range porous ordering in the material.

The electron density of silica is relatively high, which results in decent scattering of incoming X-rays. In order to increase the number of events on the detector and thereby considerably shorten the measurement time, a radiation source providing a high flux of photons is used. One such source is the synchrotron facility MAX-lab in Lund, where the SAXS analyses included in this thesis were performed (beamline I911).

5.3.1.5.4 N_2 physisorption

N_2 physisorption was used to assess the specific surface area, pore width, and pore width distribution of mesoporous silica particles. The interactions between N_2 and the silica surface is probed by controlled filling of empty pores and the first step in the analysis was therefore to degas the sample. The temperature was also lowered to 77 K prior to N_2 addition. A monolayer of nitrogen was produced on the silica surface by increasing the N_2 pressure. Monolayer data was processed using the universal gas law and the Brunauer–Emmet–Teller (BET) method to quantify the amount of adsorbed nitrogen.[94] The size and shape of the pores were subsequently assessed by increasing the N_2 pressure further until the onset of N_2 condensation (pore saturation). The pressure was then lowered to induce evaporation of nitrogen. Data obtained from this procedure was used to calculate the pore size using the Barrett–Joyner–Halenda (BJH) method.[95]

N_2 physisorption measurements were performed using a Micromeritics ASAP 2010 instrument.

5.3.2 POROUS SILICA AS AQUAPORIN-CONTAINING BILAYER SUPPORT

The use of silicon-based supports for formation of planar phospholipid bilayers was first presented by Tamm and McConnell in 1985[96] and has since been used extensively to study cell membrane models using techniques that are unsuitable for bulk preparations. This approach has been useful in studies of some membrane proteins[97-99] and offers better mechanical stability in combination with on-par protein accessibility compared to proteoliposomes in solution. Protein incorporation in SLBs does, however, suffer from the drawback of limited available space for membrane proteins underneath the bilayer. One way to create room for bulkier membrane proteins is to introduce pores in the surface of the support. Mesoporous silica has successfully been used as lipid bilayer supports, both as thin films[100] and as particles.[101] Mesoporous silica has also been used to stabilize membrane proteins, which allowed for a broader spectrum of membrane proteins to be incorporated in SLBs.[102-104] The incorporation of aquaporins in an SLB supported by mesoporous silica is of particular relevance to this thesis and presented in publication II.[105]

Formation of hAQP4-containing pSLBs on mesoporous silica films was studied using the surface sensitive analysis techniques QCM-D and total internal reflection fluorescence (TIRF) microscopy. QCM-D revealed that pSLB formation was readily accomplished on mesoporous silica, albeit taking approximately an order of magnitude longer than SLB formation on the same substrate (Fig. 9A). Proteoliposomes were also introduced to a nonporous silica substrate, whereby no pSLB formation was observed.

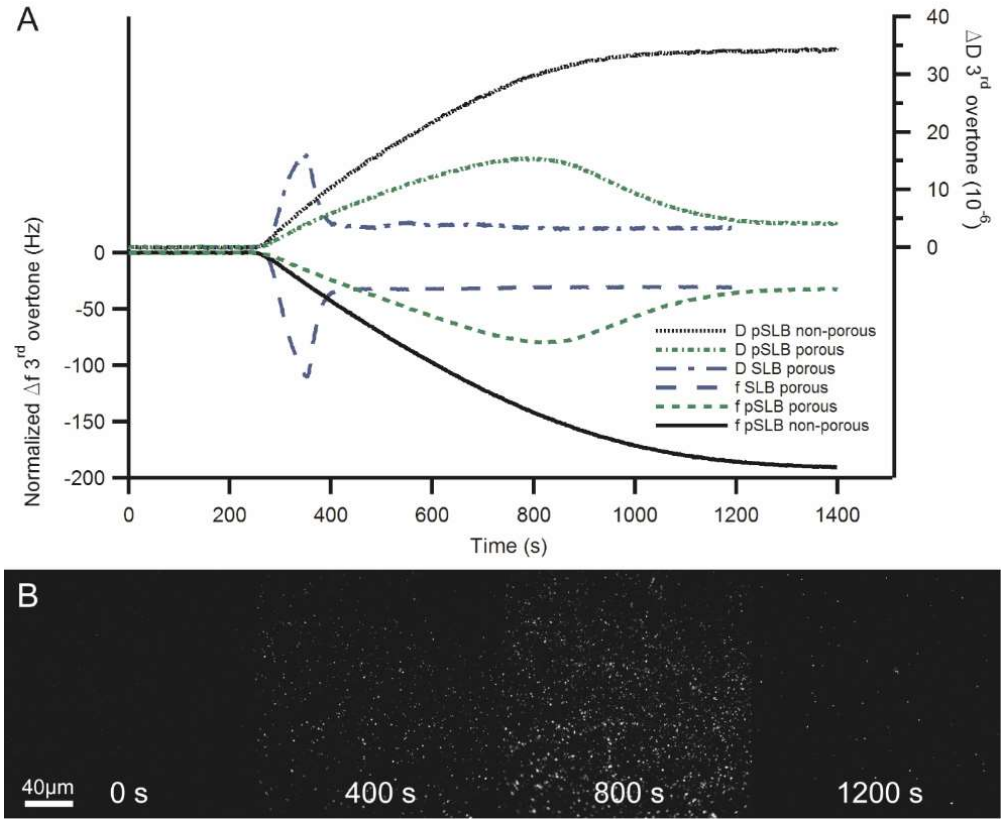

Figure 9. (A) QCM-D recording of bilayer formation processes starting from the addition of POPC liposomes and hAQP4-containing POPC proteoliposomes to nonporous and mesoporous silica. Sample was continuously added to the sensors at a flow rate of 50 μL min^{-1} throughout the measurement. The normalized frequency shift on the left axis and dissipation on the right axis are presented as a function of time. Positive y-values represent ΔD and negative y-values represent Δf for the supported lipid bilayer (SLB) formation on mesoporous silica (blue), protein-containing supported lipid bilayer (pSLB) formation on nonporous silica (black), and pSLB formation on mesoporous silica (green). (B) TIRF microscopy images showing pSLB formation on mesoporous silica as a function of time; 800 s of intact proteoliposome adsorption is seen as an increasing number of bright dots (fluorescently labeled proteoliposomes), followed by proteoliposome rupture and pSLB formation.

The hAQP4-containing pSLB formation process was also investigated using TIRF microscopy (Figure 9B), which confirmed the formation of a pSLB on mesoporous silica. Furthermore, lipid and hAQP4 diffusivity measurements were conducted using fluorescence recovery after photobleaching (FRAP) once the pSLB had been formed. The pSLB lipid diffusivity was 2.42 ± 0.04 $\mu m^2 s^{-1}$, which was slightly higher than the pSLB lipid diffusivity on nonporous silica (2.21 ± 0.07 $\mu m^2 s^{-1}$). hAQP4 was immobile on mesoporous silica, which could possibly be an effect of pore utilization. AQP4 has previously been shown to be immobile when forming orthogonal arrays in native cell membranes, [106] which could occur in our setup as well.

The formed hAQP4-containing pSLB was studied using neutron reflectivity (NR) to investigate the positioning of the organic components in relation to the mesoporous silica. Contrast matching (CM) was used to obtain different contrasts in the measurements, for example by matching the scattering length density (SLD) of the aqueous solution to the SLD of silica ($cmSiO_2$). The Bragg peak in the reflectivity profile from the mesoporous sample was present due to the long-range ordering of the pore network, which was previously assessed using SAXS (Figure 8B).

The bilayers formed on nonporous substrates did not share many common characteristics with those formed on mesoporous substrates. The major difference was that the bilayer formed on the nonporous substrate did not contain any proteins, whereas the bilayer formed on the mesoporous substrate did (Fig. 10A-D). The bilayer formed on the nonporous substrate hence consisted of POPC only. The best fit to the data was obtained by including a low coverage of additional bilayer stacks on top of the bilayer, representing the existence of co-adsorbed proteoliposomes. The bilayer surface coverage was 95 ± 5 % and the co-adsorbed proteoliposome coverage was 3 %.

The bilayer formed on the mesoporous silica substrate was very different. The bilayer surface coverage was similar at 87 ± 5 % but the hAQP4 content in the bilayer was 58 ± 5 %. There were no co-adsorbed vesicles resting on top of the pSLB. An advantage of using neutron reflectivity is its high resolution in the direction perpendicular to the substrate (on the order of a few Å), which allows differences in material composition along that direction to be probed with high accuracy. The plot of volume fraction as a function of distance from the center of the bilayer for the pSLB on mesoporous silica showed that the extracellular domains of the protein extended 10.0 ± 1.0 nm into the bulk solution (Fig. 10C). Proteins were also oriented in the opposite direction with their extracellular domains facing the substrate, where they were shown to extend 7.2 ± 1.0 nm into the mesopores. As much as 10 ± 5 % of the volume at that depth was occupied by protein, suggesting that the proteins make use of the accessible and water-filled pores of the mesoporous silica thin film to accommodate their extracellular domains.

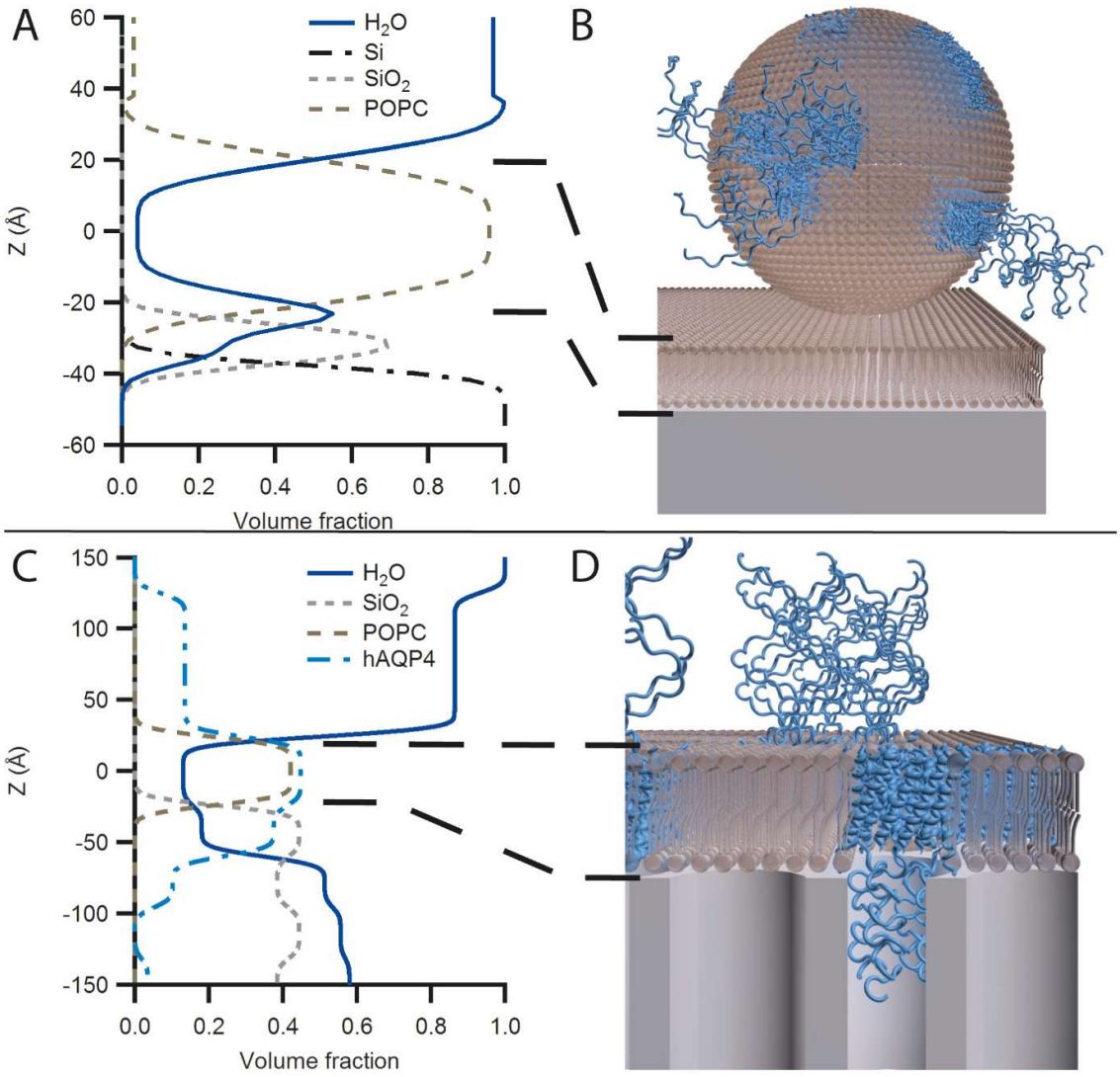

Figure 10. (A) Volume fractions corresponding to the fits for the SLB on a nonporous Si substrate (bilayer thickness = 4.6 nm). (B) Illustration visualizing the NR data for the POPC (brown) bilayer on nonporous silica (gray) with an hAQP4 (blue)-containing proteoliposome co-adsorbed on top of the bilayer. (C) Volume fractions corresponding to the fits for the pSLB on top of a mesoporous substrate deposited on a Si crystal (bilayer thickness = 4.8 nm). hAQP4 protruded 7.2 ± 1.0 nm into the porous substrate and 10.0 ± 1.0 nm into the bulk when the extracellular domains were facing the substrate and away from the substrate, respectively. (D) Illustration visualizing the NR data for the POPC (brown) bilayer containing hAQP4 (blue) intercalated with mesoporous silica (gray).

5.3.2.1 Preparation of aquaporin-containing silica-supported POPC bilayers

pSLB formation on mesoporous silica is the process in which spontaneous proteoliposome adsorption, fusion and rupture on the mesoporous silica substrate results in a pSLB. This process was straightforward both using a continuously flowing proteoliposome solution and without applying external flow. Proteoliposomes were prepared as described in section 5.2.3.1 using hAQP4 and POPC lipids. Proteoliposome diffusion and interaction with the negatively charged silica (pH 8) resulted in spontaneous proteoliposome adsorption on the surface of the mesoporous silica thin film. Continuous adsorption led to crowding of proteoliposomes on the surface, resulting in proteoliposome–proteoliposome interactions. These interactions in combination with proteoliposome–silica interactions eventually led to proteoliposome fusion and rupture, which finally resulted in pSLB formation. This process is schematically visualized in Figure 11.

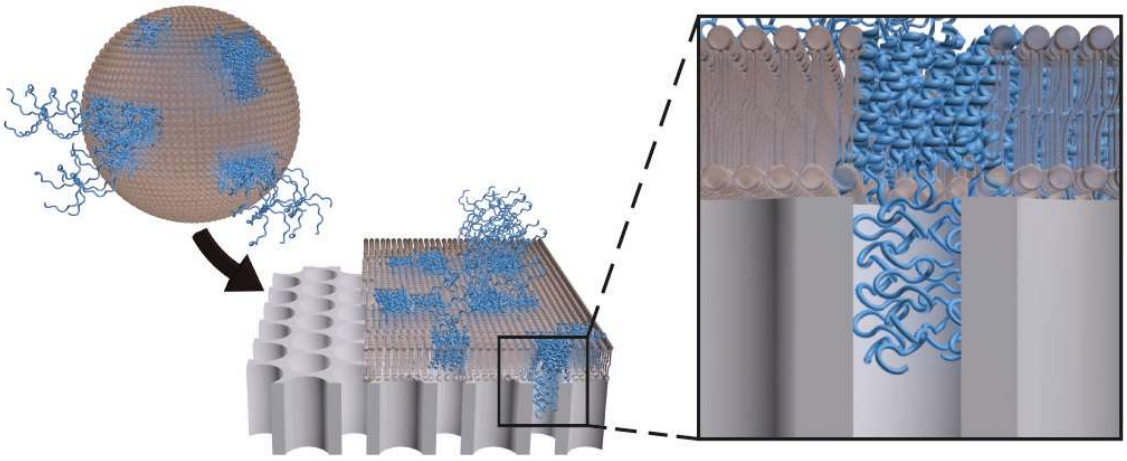

Figure 11. Schematic illustration showing the process of human aquaporin 4 (blue)-containing supported POPC (brown) bilayer formation from proteoliposomes on mesoporous silica (gray). The enlargement depicts extracellular aquaporin domains extending into a pore in the mesoporous silica.

5.3.2.2 Characterization of aquaporin-containing silica-supported POPC bilayers

The process of pSLB formation and the resulting materials were studied using surface sensitive techniques and neutron reflectivity. The analysis methods that were used provided evidence of the existence of a pSLB structure and revealed details about the process in which it was formed. The analyses also provided evidence of intercalation between the mesoporous silica and hAQP4.

5.3.2.2.1 Quartz crystal microbalance with dissipation monitoring

QCM-D was employed to study the process of pSLB formation. QCM-D is a surface sensitive technique that measures the change in oscillation frequency and the energy dissipation of an oscillating QCM-D crystal with time. The surface of interest (a mesoporous silica thin film in this thesis) is coated onto a quartz crystal that is sandwiched between two gold electrodes. An alternating voltage is applied across the crystal, resulting in an induced strain to the piezoelectric quartz crystal lattice. As a result, the crystal starts to oscillate in a shearing mode. The crystal oscillates at its acoustic resonance frequency. The measured frequency changes as mass is deposited onto the crystal, resulting in a negative Δf. Provided that the deposited matter is rigid, the observed frequency shift can be converted into deposited mass using the Sauerbrey relation

$$\Delta m = -\frac{\Delta f \times C}{n} \tag{7}$$

where Δm is the adsorbed mass, Δf is the frequency shift, C is the mass sensitivity constant (17.7 ng Hz^{-1} cm^{-2}), and n is the overtone number. In addition to the deposited mass, QCM-D also assesses the viscoelastic properties of the adsorbed matter by monitoring the dampening in the system upon deposition.

QCM-D results presented in this thesis were obtained using a QCM-D E4 (Biolin Scientific) system coupled to a peristaltic pump.

5.3.2.2.2 Total internal reflection fluorescence microscopy

TIRF microscopy was used as a complementary method to QCM-D for studying the pSLB formation process. TIRF microscopy is a branch of fluorescence microscopy, which in turn is a branch of optical microscopy. Optical microscopy uses visible light to image objects that are magnified using optics. The limitation of optical microscopy is the diffraction barrier using visible light, which resides at approximately half the wavelength of the light used to image the object. The pSLB presented in this thesis is ~5 nm thick, which is much smaller than the Abbe diffraction limit of visible light (~150 nm) and therefore cannot be imaged using regular optical microscopy.

Fluorescence microscopy is a means of imaging small entities using optical microscopy. The lipids and proteins used in this thesis are not inherently fluorescent and therefore need to be labeled with a fluorescent dye for this to be possible. A

fluorescent dye is a molecule in which electrons can be excited to a higher energy level by the absorption of incoming photons that match the band gap between the excited state and the ground state. The excited state is however not stable and excited electrons are forced into a lower and more stable energy state in the process of relaxation. Electrons do not always go back to the ground state but rather to an intermediate state, which corresponds to a smaller energy gap and hence a longer wavelength compared to that used to excite the electron in the first place. The benefit of this is that the specific fluorescence wavelength can be isolated from the illumination wavelengths using filters, which allows specific detection of fluorescent molecules at high spatial resolution.

TIRF microscopy is used to specifically image fluorescent entities close to a surface and is therefore useful in studies of substrate-supported planar membranes.[107] Above a certain critical angle normal to the substrate, incoming light may be totally reflected if it is propagating from a material of higher refractive index (RI) towards a material of lower refractive index. As totally internally reflected light is propagating through the substrate, an evanescent field is present at the interface between the substrate surface and for example a liquid sample. The evanescent field decays exponentially with the distance from the surface in the direction perpendicular to the surface. Hence, the evanescent field only reaches roughly 100 nm into the bulk, which renders it suitable for probing sample-surface interactions.

The TIRF microscopy setup used in this thesis was inverted, meaning that the substrate–liquid interface was imaged from below, through the transparent glass substrate. A Nikon Eclipse Ti-E microscope equipped with an Andor Ixon+ camera and a 60× oil immersion objective was used.

5.3.2.2.3 Fluorescence recovery after photobleaching

FRAP[108, 109] was used to indirectly assess the fluidity of lipids and proteins in the pSLB through determining the diffusion of fluorescent molecules attached to these species. In the FRAP analyses presented in this thesis, TIRF microscopy (section 5.3.2.2.2) was used to visualize movement of fluorescent molecules upon bleaching a well-defined pSLB area using a high intensity laser. After bleaching, fluorophores coupled to lipids situated inside the bleached area diffuse out whereas lipids connected to fluorophores that were not bleached diffuse into the bleached spot, which leads to recovery of the homogeneously fluorescent bilayer. The recovery was monitored by time lapse imaging from which a diffusion coefficient was deduced.

FRAP results presented in this thesis were collected using a Nikon Eclipse Ti-E microscope equipped with an Andor Ixon+ camera.

5.3.2.2.4 Neutron reflectivity

NR was used to study the organic–inorganic interface in detail. The wavelengths of the employed neutrons are typically in the range of 0.2-1.0 nm and highly resolved material data was therefore obtained using neutrons. Since neutrons are neutrally charged, they do not interact electrostatically with protons and electrons, which allows them to non-destructively penetrate deep into materials.

In the NR study presented in this thesis (Publication II), neutrons were approaching the mesoporous silica thin film and the pSLB through a single-crystal silicon block. As they encountered an interface they were reflected at an angle θ if the encountered material had a higher SLD than the material that the neutrons approached the interface from. Interactions of neutrons with atomic nuclei render NR sensitive to isotopic differences, such as the one neutron difference between hydrogen and deuterium. Isotopic substitution is therefore commonly used in NR to increase the contrast between the entity of interest and the surroundings. In this thesis, H_2O was fully or partially substituted for D_2O in some measurements to alter the contrast of aquaporins and lipids to silica and water. In addition, contrast matching by isotopic substitution was performed to provide complementary data sets for modelling.

The NR experiments presented in this thesis were conducted at the SURF reflectometer at ISIS, STFC Rutherford Appleton Laboratory (Didcot, UK).[110, 111] At this site, neutrons are produced through spallation in which neutrons are released by firing high-energy protons into a tungsten target. Proton bombardment induces nuclear reactions in the tungsten target that results in the emission of neutrons.

5.3.3 SILICIFICATION

Silicification is the process of immobilizing an entity using silica. This can be done in different ways, for example through encapsulation,[112] filling,[113] or coating.[114] Encapsulation of soluble proteins in a silica matrix has been shown to improve protein characteristics such as thermal, chemical, and mechanical stability while preserving functionality.[115-117] This thesis presents work in which the application of a silica coating was used for stabilization, reasoning that it would result in higher mass transport compared to silica encapsulation while providing sufficient stabilization.

5.3.3.1 Silicification of aquaporin-containing lipid bilayers

As mentioned previously in this thesis, membrane proteins are typically reconstituted into cell membrane mimics for use in applications that demand protein functionality.[31, 118] Liposomes are spherical lipid bilayer constructs that offer a native-like, yet well-defined model system commonly used for membrane protein reconstitution.[119] They are, however, typically not stable enough for prolonged use in demanding applications. For example, the use of lipid bilayers in applications like wastewater treatment is complicated due to the poor rejection of hydrophobic particles and other contaminants offered by the exposed lipid bilayer.[18]

An interesting lipid bilayer stabilization approach was introduced by Bégu and coworkers, who deposited a thin silica coating on liposomes.[114, 120] The use of this approach for proteoliposome stabilization should benefit from higher mass transport in comparison to proteoliposome encapsulation and therefore be of interest in applications such as water purification. The current struggle to combine high water flux with high selectivity results in high energy consumptions of for instance desalination, which was mentioned earlier.[14]

Work presented in publication III investigated the formation process in which silica-coated hAQP4-containing proteoliposomes were formed. Small-angle neutron scattering (SANS) was used to study the formation process. The short wavelength of neutrons allowed for detailed structural characterization of POPC liposomes and proteoliposomes with an emphasis on the structure of the bilayer and the effect of silica introduction. The formation of the silica layer itself was also studied with great interest. The SANS characterization of the hAQP4-containing proteoliposome silicification process is presented in Figure 12A. Gradual changes in scattering are clearly seen with time as the silicification process proceeds through precursor hydrolysis and subsequent condensation into silica as described in equations 3-5. Prior to silicification, liposomes and proteoliposomes were characterized in multiple solvent contrasts with data spanning a wider q-range than during the formation process in order to provide solid complementary data sets for modelling (publication III).

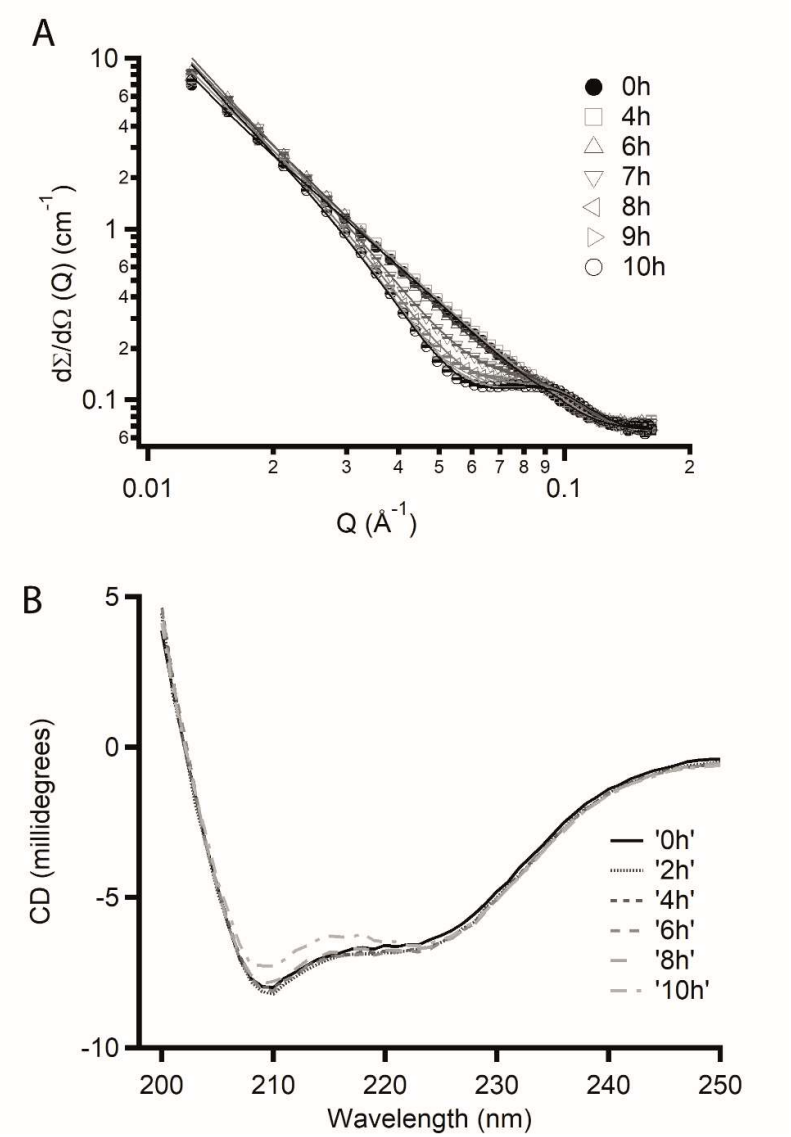

Figure 12: (A) SANS profiles showing the hAQP4-containing proteoliposome silicification process. (B) CD spectra of hAQP4 during proteoliposome silicification presented in 2h increments.

Circular dichroism (CD) was used to study the aquaporin structure throughout the proteoliposome silicification process. CD probes the differential absorption of right-handed and left-handed circularly polarized light, which makes it a suitable method to assess the secondary structure of proteins. Since aquaporins consist of six transmembrane α-helices and a seventh pseudo α-helix they are clearly detected as having an α-helical footprint. The data presented in this thesis did indeed show the characteristic α-helix footprint as seen in Figure 12B. Moreover, the collection of CD data throughout the process of proteoliposome silicification revealed that the secondary structure of the proteins was retained upon the formation of the silica shell.

The SANS data was modelled to provide a description of the silica formation process on POPC liposomes and hAQP4-containing proteoliposomes. The model included the structural parameters presented in Figure 13A in addition to the proteoliposome radius. The full set of modelling parameters is found in publication III. The model revealed that the silica-shell formation started by the arrangement of dilute silica on the outer bilayer leaflet for both liposomes and proteoliposomes. This layer was densified with time by the expulsion of buffer and further silica condensation. The change in deposited silica volume with time is presented in Figure 13B. As can be seen from the figure, the formation process is similar on liposomes and proteoliposomes with the exception that there is a delay in the onset of proteoliposome silicification. This delay was suggested to be caused primarily by steric hindrance introduced by aquaporin insertion, preventing the silicic acid species from interacting with the lipid bilayer.

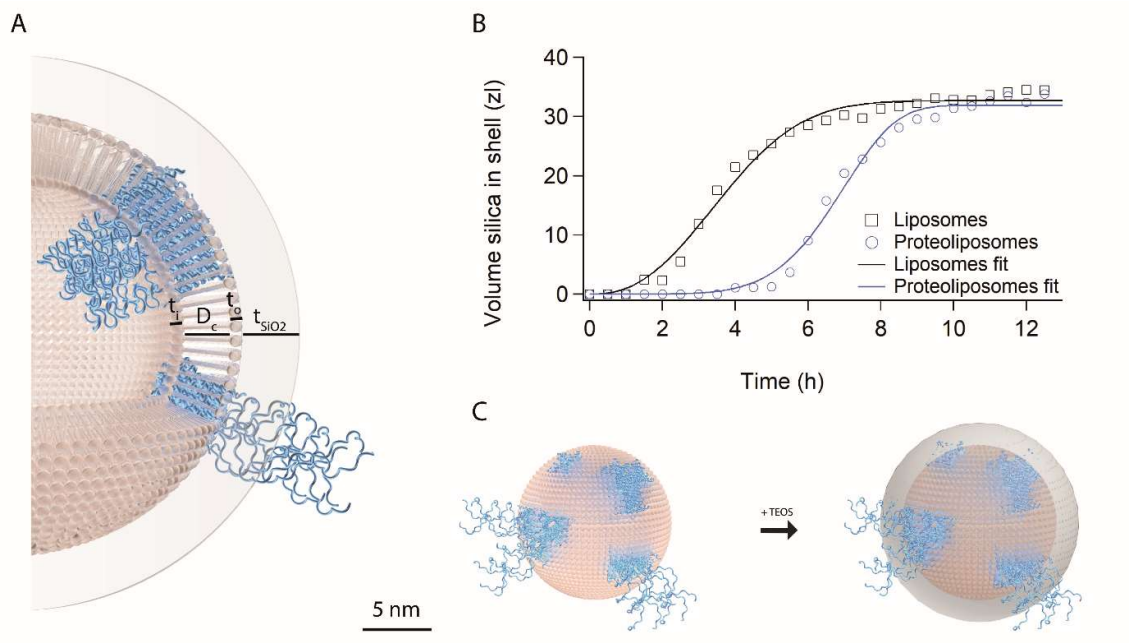

Figure 13: (A) Illustration depicting a partly opened silicified hAQP4-containing proteoliposome with geometrical parameters assigned. t_i represents the thickness of the inner leaflet lipid headgroups, D_c represents the thickness of the hydrophobic lipid tails from both leaflets, t_o represents the thickness of the outer leaflet lipid headgroups, and t_{SiO2} represents the thickness of the silica shell. hAQP4 is depicted in blue, POPC lipids in brown, and silica in gray. (B) Comparison of deposited silica volumes as a function of time for liposome (black) and proteoliposome (blue) silicification. The solid lines present fits to an Avrami-type equation. (C) Schematic illustration of the silicification process. hAQP4-containing proteoliposomes are mixed with the silica precursor TEOS, which results in the formation of a silica shell on the outside of the proteoliposome. Colors according to (A).

The silicified samples were dried and analyzed by different modes of TEM to obtain additional structural and compositional data on silicified liposomes and proteoliposomes. TEM micrographs of silicified POPC liposomes and hAQP4-containing POPC proteoliposomes are depicted in Figure 14A and B, respectively. The samples retain their spherical shape to varying extents, which is likely due to interactions during the silicification process and perhaps also in sample drying. Both samples are clearly aggregated, as was also observed when studying the formation process using SANS and CD.

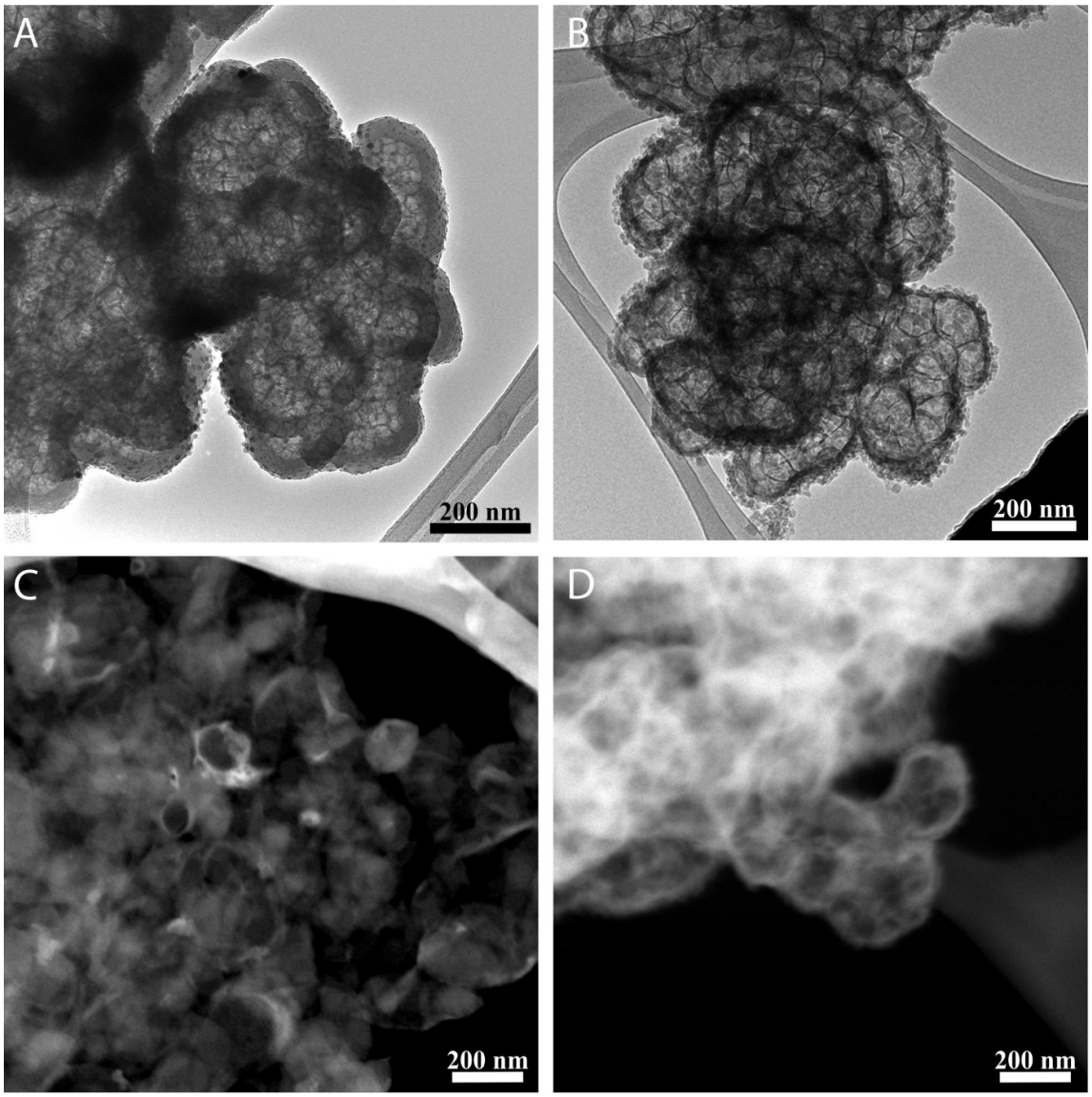

Figure 14: Bright field TEM micrographs of (A) silicified liposomes and (B) silicified proteoliposomes obtained after complete silicification. The dark lines depict the hydrocarbon tails of lipid bilayers whereas the gray areas in connection to the hydrocarbon tails consist of silica. STEM micrographs of (C) silicified liposomes and (D) silicified proteoliposomes obtained after complete silicification. Silica exhibits a bright contrast.

Scanning transmission electron microscopy (STEM) was used as a complement to TEM to locate silica deposition in silicified liposome and proteoliposome samples (Fig. 14C and D, respectively). Silica is seen as bright features lining the liposomes and proteoliposomes. Further investigation into the location of different elements was conducted using spectroscopic techniques. Elemental maps obtained using STEM energy-dispersive X-ray spectroscopy (EDX) on silicified hAQP4-containing proteoliposomes are presented in Figure 15 alongside a STEM high-angle annular dark-field (HAADF) micrograph of the same sample area. Silicon, carbon, oxygen, and phosphorous are clearly enriched along the border of the proteoliposomes, which was expected from the SANS model. Sulfur is only present in small amounts in the aquaporins and therefore resulted in a weak trace. Nitrogen was not detected using STEM-EDX despite being more abundant than sulfur, which is due to nitrogen being a lighter element and therefore not as readily detected by STEM-EDX.

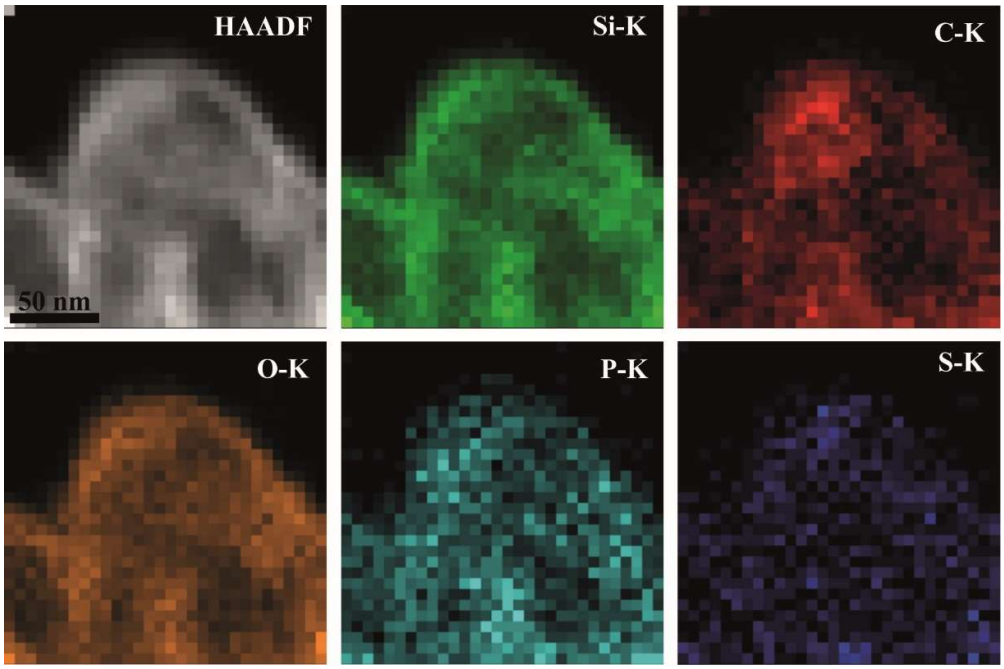

Figure 15: STEM-HAADF micrograph (top left) and corresponding elemental maps of silicified hAQP4-containing POPC proteoliposomes obtained using STEM-EDX. The K-lines of silicon (green), carbon (red), oxygen (orange), phosphorous (cyan), and sulfur (blue) are presented. All elements are enriched in the silicified bilayers lining the proteoliposomes.

Chemical mapping of silicified hAQP4-containing proteoliposomes was also performed using energy filtered (EF) TEM which is more sensitive to light elements than STEM-EDX. As seen in Figure 16, EFTEM detected all elements that were expected to be present in the sample. All elements were enriched along the proteoliposome edges, which confirmed the view presented by the STEM-EDX data.

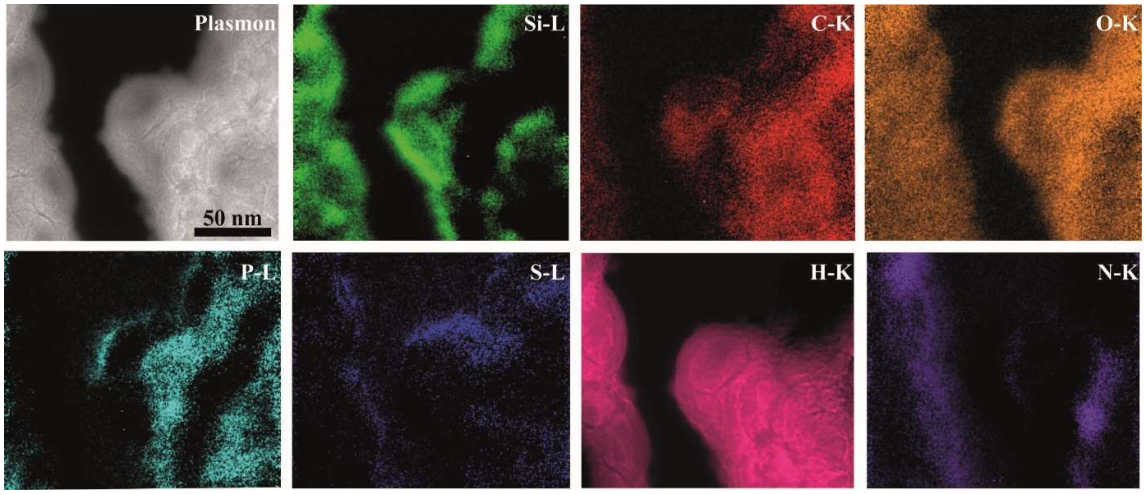

Figure 16: EFTEM images showing the plasmon filtered image (top left) and the corresponding elemental maps of silicified hAQP4-containing POPC proteoliposomes. Selected K-edges of carbon (red), oxygen (orange), hydrogen (magenta), and nitrogen (purple) are depicted alongside selected L-edges of silicon (green), phosphorous (cyan), and sulfur (blue).

5.3.3.2 Preparation of silicified aquaporin-containing POPC proteoliposomes

The silicification protocol used in publication III produced a thin layer of silica on the outside of liposomes and proteoliposomes. The proteoliposomes that were used as templates were prepared as described in section 5.2.3.1 using hAQP4 and POPC lipids. The silicon alkoxide TEOS was added to proteoliposomes in Tris buffer (pH 8). Silicon alkoxide hydrolysis (eq. 3) is acid and base-catalyzed, which results in slow hydrolysis at pH 8. Silica shells started to form after the hydrolysis had progressed to a certain level. Silicified proteoliposomes started to aggregate into larger clusters during silica condensation. The silicified proteoliposome aggregates were either kept in solution or dried, depending on how they were going to be characterized.

5.3.3.3 Characterization of silicified aquaporin-containing POPC proteoliposomes

Characterization of the silica-coated hAQP4-containing POPC proteoliposomes was performed using various modes of TEM (described in section 5.3.1.5.2) to study the positioning of the organic and inorganic components in relation to each other. SANS and CD were utilized to study the silica formation process in order to monitor structural features of the proteoliposomes and the aquaporins, respectively.

5.3.3.3.1 Small-angle neutron scattering

SANS was used to monitor the structure of liposomes and proteoliposomes throughout the process of silica formation. Neutrons interact with atomic nuclei potential and are therefore sensitive to isotopic content. This is one of the major advantages of SANS over SAXS (presented in section 5.3.1.5.3), the other being the sensitivity to light elements.[93] During analysis, the sample is exposed to a neutron beam comprising neutrons of a specific wavelength (λ=0.2-1.0 nm are typically used) to resolve structural features. Incoming (primary) neutrons interact with sample nuclei and scatter elastically. The neutrons that are elastically scattered to small angles (close to the primary beam) provide structural information about the sample. A 2D area detector is typically employed to monitor scattering intensity as a function of the momentum transfer q.

The SANS results presented in this thesis were collected in experiments conducted at the D11 instrument in ILL (Institut Laue-Langevin, Grenoble, France) and at the KWS-1 instrument in FRM-II (Research neutron source Heinz-Meier Leibnitz, Garching, Germany).

5.3.3.3.2 Circular dichroism

CD was used to monitor the aquaporin secondary structure throughout the process of proteoliposome silicification. The CD analysis technique is based on differential absorption of left and right-handed circularly polarized light, which are the components of plane polarized light. Differences in the absorption of left and right-handed circularly polarized light arise when plane polarized light passes through a chiral molecule since this molecule absorbs either the left or right-handed component to a larger extent than the other. The chromophores of interest in proteins include peptide bonds (absorption ~240-180 nm), aromatic amino acid side chains (absorption ~320-260 nm), and disulphide bonds (~260 nm). Secondary protein structure is probed by monitoring the peptide bonds, which was done in publication III in this thesis. The assessment of secondary structure is based on peptide bond absorption, which is composed of a broader $n \rightarrow \pi^*$ transition centered around 220 nm and a more specific $\pi \rightarrow \pi^*$ transition around 190 nm. Each type of secondary protein structure show a characteristic footprint in CD, such as the aquaporin α-helices probed in this thesis.[121, 122] The characteristic α-helix footprint

was slightly altered upon insertion into proteoliposomes as previously observed.[123, 124]

CD results presented in this thesis were obtained using a Chirascan™ circular dichroism spectrometer with a Peltier temperature controller.

5.3.3.3.3 Scanning transmission electron microscopy

STEM was employed in order to localize silica deposition in the silicified liposome and proteoliposomes samples. As the name implies it can be viewed as a combination of SEM and TEM. A finely focused electron beam scans a thin sample and the transmitted electrons are detected. By correlating the detector signal with the position of the electron beam, a virtual image of the analyzed sample is created. Transmitted electrons that are scattered at a relatively high angle can be detected using a HAADF detector. STEM analyses were performed using a FEI Titan 80-300 operated at 300 kV and a FEI Tecnai TF20 operated at 200 kV.

STEM was also employed for elemental mapping. The bombardment of electrons results in the emission of X-rays from the sample. These X-rays are characteristic for the elemental composition of the sample and the use of a scanning electron beam in STEM-EDX allows for elemental mapping of the specimen. STEM-EDX elemental mapping was performed using a FEI Titan 80-300 operating at 300 kV.

Elemental mapping was also performed using EFTEM. In EFTEM, electrons of specific energies can be selected (or filtered) with the use of an energy filter (a Gatan Image Filter (GIF) was used for experiments in this thesis) to come through the spectrometer, and both image and diffraction patterns can be formed. GIF is a post-column Gatan Parallel EELS detector with an energy-selecting slit after the spectrometer's magnetic prism, combined with a 2D slow-scan CCD detector. To form the filtered image, the energy spectrum has to be shifted so that the desired energy window passes through the slit. The images are using the intensity of the ionization edges of specific elements, so the images correspond to an elemental map. The three-window method was used to form the maps presented in this thesis. Three images were acquired from electrons in selected energy windows of which two images corresponded to the background before the edge and the third was a post-edge image. The background from the pre-edge images was subtracted from the post-edge image, which resulted in a quantitative image of the selected elemental distribution. EFTEM experiments were conducted using a FEI Titan 80-300 operated at 300 kV in TEM mode.

6 Concluding remarks

As stated in the very beginning of this thesis, clean drinking water is a prerequisite for life. It is therefore horrifying that the extent of water pollution is allowed to increase in times of major technological advancements in other application areas. The work presented in this thesis was part of a strive to advance water treatment technology. The steps taken so far were described in chapter 5 and this chapter provides a summary thereof.

The lack of technology that can purify our increasingly polluted water to reasonable costs is a major global concern and the ultimate driving force for the efforts undertaken within this PhD project. After careful consideration of which approach to use to take on the massive task of developing improved purification technology, the biomimetic approach was deemed the most promising. Since a lot of potential associated with biomimetic water purification was tied to the unique combination of high selectivity and flux possessed by aquaporins, the use of aquaporins in a filter setting was chosen as the path forward. The main drawback of such designs that had been tested to date was the limited aquaporin stability in synthetic filter environments. This was where we decided to put our focus. We decided to investigate the possibilities of stabilizing aquaporins using naturally abundant silica by *housing aquaporins in nanostructured glass*. Below is a summary of how far we have reached.

The developed stabilization approaches used in this work were presented in a general manner in this thesis. Detailed procedures are found in the publications on which the thesis is based. The common denominator of the stabilization approaches was the use of aquaporins that were incorporated in native-like lipid bilayers and stabilized by silica. Two main designs were developed:

- Aquaporins in supported lipid bilayers on mesoporous silica substrates
- Aquaporins in proteoliposomes coated by a thin layer of silica

The first approach resulted in the synthesis of mesoporous silica particles having different pore characteristics. The most promising particle for protein stabilization purposes had pore widths in the range of ~6-14 nm. The mesoporous silica

stabilization approach did, however, proceed into using planar mesoporous substrates before the particles had been used in stabilization trials.

Mesoporous silica thin film development included the use of different pore templating agents and protocols to tune the pore size and pore arrangement of the thin films. The purpose of the silica was to stabilize aquaporins and the pore size and pore arrangement were therefore tuned to match the natural aquaporin packing behavior. The final silica thin film had pore diameters of 6 nm that were hexagonally arranged and accessible from the surface. Aquaporin-containing proteoliposomes were introduced to these substrates and spontaneously formed aquaporin-containing supported lipid bilayers resting on top of the silica. The extracellular aquaporin domains were shown to utilize the aqueous space provided by the pores underneath the bilayer, which were key to form an aquaporin-supported lipid bilayer from aquaporin-containing proteoliposomes.

The second stabilization approach started to gain attention about halfway into the project following some promising trials on liposome silicification. Proteoliposome silicification protocols were developed and tested, varying parameters such as pH, prehydrolysis time, and temperature of the silicification process. Previous studies on liposome silicification using TEOS as silica precursor indicated that the ethanol released in the process could damage the lipid bilayer. It was therefore of interest to study the formation process in detail to elucidate the effect of silicification on the aquaporin-containing proteoliposomes. This turned out to be a challenging task since silicified proteoliposomes aggregated during the silicification process, which eventually resulted in sedimentation. Analysis procedure optimizations eventually resulted in an interesting description on the build-up of the silica shell. Modelling showed that the silica shell was not continuously increasing in thickness with time, but that there was an initial arrangement of very dilute silica on the outside of the proteoliposome followed by silica condensation. The shell therefore became slightly thinner with time, albeit denser. The characteristics of the templating proteoliposome did basically not change except for the swelling of the outer leaflet headgroups. Importantly, aquaporins were shown to retain their secondary structure upon silicification. The silicified samples were also dried and analyzed using electron microscopy and elemental mapping to assess the stability of the samples and the spatial distribution of compounds upon silicification. Silicon was shown to be preferentially located at proteoliposome borders along with elements specific to lipids and aquaporins, indicating successful silicification of intact proteoliposomes.

The work summarized so far used human aquaporin 4 for reasons explained in section 5.1.1. Studies on the climbing perch aquaporin 1 were conducted due to its suggested involvement in the extraordinary environmental adaptability of the fish climbing perch. This aquaporin was structurally and functionally characterized, which revealed a novel fold that was suggested to act as a channel blocker, closing the water channel when needed. Human aquaporin 4 does not possess this functionality which could potentially be utilized to regulate water flux. Silica stabilization of this aquaporin was not pursued in this thesis.

In summary, the results show that it is possible to stabilize human aquaporin 4 by using mesoporous planar silica supports or by applying a silica coating. Mesoporous silica particles were synthesized as an alternative to thin films whereas climbing perch aquaporin 1 was investigated as a possible alternative to human aquaporin 4.

7 Future perspectives

Does this thesis purify water? No, it does not. There are, however, nuances in this thesis that may become useful in our joint efforts to clean up the Earth. The greatest societal contribution of most PhD projects is the creation and spreading of knowledge and my hope is that the knowledge disseminated through this thesis will be used to sustainably purify water. Biomimetic water filtration shows great promise and successful aquaporin stabilization might be the silver bullet that makes it flourish.

The next step on the journey towards highly selective and energy-efficient water treatment is to evaluate these stabilization strategies in real-world applications. This will be my next challenge and I am very excited to see if this is one piece of the puzzle that will bring about a bright blue new dawn.

Figure 17. Dawn approaching [Photo credit: NASA]

References

1. Khetan, S. K.; Collins, T. J. *Chem. Rev.* **2007,** 107, (6), 2319-2364.
2. Cockell, C. S. *Nature* **2009,** 457, (7225), 30-30.
3. Petsko, G. A. *Genome Biol.* **2011,** 12, (4), 3.
4. Giwa, A.; Hasan, S. W.; Yousuf, A.; Chakraborty, S.; Johnson, D. J.; Hilal, N. *Desalination* **2017,** 420, 403-424.
5. Massoud, E. C.; Purdy, A. J.; Miro, M. E.; Famiglietti, J. S. *Sci Rep* **2018,** 8, 9.
6. Micklin, P., The Aral Sea disaster. In *Annual Review of Earth and Planetary Sciences*, Annual Reviews: Palo Alto, 2007; Vol. 35, pp 47-72.
7. Vitousek, P. M.; Mooney, H. A.; Lubchenco, J.; Melillo, J. M. *Science* **1997,** 277, (5325), 494-499.
8. Schwarzenbach, R. P.; Escher, B. I.; Fenner, K.; Hofstetter, T. B.; Johnson, C. A.; von Gunten, U.; Wehrli, B. *Science* **2006,** 313, (5790), 1072-1077.
9. Cole, M.; Lindeque, P.; Halsband, C.; Galloway, T. S. *Mar. Pollut. Bull.* **2011,** 62, (12), 2588-2597.
10. Doney, S. C. *Science* **2010,** 328, (5985), 1512-1516.
11. *Progress on Drinking Water, Sanitation and Hygiene: 2017 update and SDG baselines*; WHO, unicef, 2017.
12. *Human Rights Obligations Related to Access to Safe Drinking Water and Sanitation*; UN, 2010.
13. *Transforming Our World: The 2030 Agenda for Sustainable Development*; United Nations General Assembly Resolution, A/RES/70/1: 2015.
14. Werber, J. R.; Osuji, C. O.; Elimelech, M. *Nat. Rev. Mater.* **2016,** 1, (5), 16.
15. Elimelech, M.; Phillip, W. A. *Science* **2011,** 333, (6043), 712-717.
16. Geise, G. M.; Paul, D. R.; Freeman, B. D. *Prog. Polym. Sci.* **2014,** 39, (1), 1-42.
17. Al-Karaghouli, A.; Kazmerski, L. L. *Renew. Sust. Energ. Rev.* **2013,** 24, 343-356.
18. Werber, J. R.; Elimelech, M. *Sci. Adv.* **2018,** 4, (6), 9.
19. Caroni, P.; Zurini, M.; Clark, A.; Carafoli, E. *J. Biol. Chem.* **1983,** 258, (12), 7305-7310.
20. Breitwieser, G. E.; Szabo, G. *J. Gen. Physiol.* **1988,** 91, (4), 469-493.

21. Preston, G. M.; Carroll, T. P.; Guggino, W. B.; Agre, P. *Science* **1992,** 256, (5055), 385-387.

22. Benga, G.; Popescu, O.; Pop, V. I.; Holmes, R. P. *Biochemistry* **1986,** 25, (7), 1535-1538.

23. Denker, B. M.; Smith, B. L.; Kuhajda, F. P.; Agre, P. *J. Biol. Chem.* **1988,** 263, (30), 15634-15642.

24. King, L. S.; Kozono, D.; Agre, P. *Nat. Rev. Mol. Cell Biol.* **2004,** 5, (9), 687-698.

25. Ishibashi, K.; Hara, S.; Kondo, S. *Clin. Exp. Nephrol.* **2009,** 13, (2), 107-117.

26. Chen, H. N.; Ilan, B.; Wu, Y. J.; Zhu, F. Q.; Schulten, K.; Voth, G. A. *Biophys. J.* **2007,** 92, (1), 46-60.

27. Ho, J. D.; Yeh, R.; Sandstrom, A.; Chorny, I.; Harries, W. E. C.; Robbins, R. A.; Miercke, L. J. W.; Stroud, R. M. *Proc. Natl. Acad. Sci. U. S. A.* **2009,** 106, (18), 7437-7442.

28. Eriksson, U. K.; Fischer, G.; Friemann, R.; Enkavi, G.; Tajkhorshid, E.; Neutze, R. *Science* **2013,** 340, (6138), 1346-1349.

29. Huisman, L.; Wood, W. E. *Slow sand filtration*; WHO, 1974.

30. Bhushan, B. *Philos. Trans. R. Soc. A-Math. Phys. Eng. Sci.* **2009,** 367, (1893), 1445-1486.

31. Booth, P. J. *Biochim. Biophys. Acta-Biomembr.* **2003,** 1610, (1), 51-56.

32. Kaufman, Y.; Berman, A.; Freger, V. *Langmuir* **2010,** 26, (10), 7388-7395.

33. Li, X. S.; Wang, R.; Tang, C. Y.; Vararattanavech, A.; Zhao, Y.; Torres, J.; Fane, T. *Colloid Surf. B-Biointerfaces* **2012,** 94, 333-340.

34. Sun, G. F.; Chung, T. S.; Jeyaseelan, K.; Armugam, A. *Colloid Surf. B-Biointerfaces* **2013,** 102, 466-471.

35. Stoenescu, R.; Graff, A.; Meier, W. *Macromol. Biosci.* **2004,** 4, (10), 930-935.

36. Kumar, M.; Grzelakowski, M.; Zilles, J.; Clark, M.; Meier, W. *Proc. Natl. Acad. Sci. U. S. A.* **2007,** 104, (52), 20719-20724.

37. Wang, H. L.; Chung, T. S.; Tong, Y. W.; Jeyaseelan, K.; Armugam, A.; Chen, Z. C.; Hong, M. H.; Meier, W. *Small* **2012,** 8, (8), 1185-1190.

38. Kumar, M.; Habel, J. E. O.; Shen, Y. X.; Meier, W. P.; Walz, T. *J. Am. Chem. Soc.* **2012,** 134, (45), 18631-18637.

39. Duong, P. H. H.; Chung, T. S.; Jeyaseelan, K.; Armugam, A.; Chen, Z. C.; Yang, J.; Hong, M. H. *J. Membr. Sci.* **2012,** 409, 34-43.

40. Zhong, P. S.; Chung, T. S.; Jeyaseelan, K.; Armugam, A. *J. Membr. Sci.* **2012,** 407, 27-33.

41. Wang, H. L.; Chung, T. S.; Tong, Y. W.; Jeyaseelan, K.; Armugam, A.; Duong, H. H. P.; Fu, F. J.; Seah, H.; Yang, J.; Hong, M. H. *J. Membr. Sci.* **2013,** 434, 130-136.

42. Xie, W. Y.; Low, J. W. J.; Armugam, A.; Jeyaseelan, K.; Tong, Y. W. *AIMS Biophys.* **2015,** 2, (3), 381-397.

43. Kaufman, Y.; Grinberg, S.; Linder, C.; Heldman, E.; Gilron, J.; Shen, Y. X.; Kumar, M.; Lammertink, R. G. H.; Freger, V. *J. Membr. Sci.* **2014,** 457, 50-61.

44. He, Y.; Hoi, H.; Abraham, S.; Montemagno, C. D. *J. Appl. Polym. Sci.* **2018,** 135, (15), 7.

45. He, Y.; Hoi, H. F.; Montemagno, C. D.; Abraham, S. *J. Appl. Polym. Sci.* **2018,** 135, (35), 6.

46. Li, X. S.; Chou, S. R.; Wang, R.; Shi, L.; Fang, W. X.; Chaitra, G.; Tang, C. Y. Y.; Torres, J.; Hu, X.; Fane, A. G. *J. Membr. Sci.* **2015,** 494, 68-77.

47. Sengur-Tasdemir, R.; Sayinli, B.; Urper, G. M.; Tutuncu, H. E.; Gul-Karaguler, N.; Ates-Genceli, E.; Tarabara, V. V.; Koyuncu, I. *New J. Chem.* **2018,** 42, (21), 17769-17778.

48. Hummer, G.; Rasaiah, J. C.; Noworyta, J. P. *Nature* **2001,** 414, (6860), 188-190.

49. Geng, J.; Kim, K.; Zhang, J. F.; Escalada, A.; Tunuguntla, R.; Comolli, L. R.; Allen, F. I.; Shnyrova, A. V.; Cho, K. R.; Munoz, D.; Wang, Y. M.; Grigoropoulos, C. P.; Ajo-Franklin, C. M.; Frolov, V. A.; Noy, A. *Nature* **2014,** 514, (7524), 612-615.

50. Kim, K.; Geng, J.; Tunuguntla, R.; Comolli, L. R.; Grigoropoulos, C. P.; Ajo-Franklin, C. M.; Noy, A. *Nano Letters* **2014,** 14, (12), 7051-7056.

51. Tunuguntla, R. H.; Henley, R. Y.; Yao, Y. C.; Pham, T. A.; Wanunu, M.; Noy, A. *Science* **2017,** 357, (6353), 792-796.

52. Sanborn, J. R.; Chen, X.; Yao, Y. C.; Hammons, J. A.; Tunuguntla, R. H.; Zhang, Y. L.; Newcomb, C. C.; Soltis, J. A.; De Yoreo, J. J.; Van Buuren, A.; Parikh, A. N.; Noy, A. *Adv. Mater.* **2018,** 30, (51), 9.

53. Fei, Z. F.; Zhao, D. B.; Geldbach, T. J.; Scopelliti, R.; Dyson, P. J.; Antonijevic, S.; Bodenhausen, G. *Angew. Chem.-Int. Edit.* **2005,** 44, (35), 5720-5725.

54. Zhou, X. B.; Liu, G. D.; Yamato, K.; Shen, Y.; Cheng, R. X.; Wei, X. X.; Bai, W. L.; Gao, Y.; Li, H.; Liu, Y.; Liu, F. T.; Czajkowsky, D. M.; Wang, J. F.; Dabney, M. J.; Cai, Z. H.; Hu, J.; Bright, F. V.; He, L.; Zeng, X. C.; Shao, Z. F.; Gong, B. *Nat. Commun.* **2012,** 3, 8.

55. Le Duc, Y.; Michau, M.; Gilles, A.; Gence, V.; Legrand, Y. M.; van der Lee, A.; Tingry, S.; Barboiu, M. *Angew. Chem.-Int. Edit.* **2011,** 50, (48), 11366-11372.

56. Jeon, H. G.; Jung, J. Y.; Kang, P.; Choi, M. G.; Jeong, K. S. *J. Am. Chem. Soc.* **2016,** 138, (1), 92-95.

57. Shen, Y. X.; Song, W. C.; Barden, D. R.; Ren, T. W.; Lang, C.; Feroz, H.; Henderson, C. B.; Saboe, P. O.; Tsai, D.; Yan, H. J.; Butler, P. J.; Bazan, G. C.; Phillip, W. A.; Hickey, R. J.; Cremer, P. S.; Vashisth, H.; Kumar, M. *Nat. Commun.* **2018,** 9, 11.

58. Wedepohl, K. H. *Geochim. Cosmochim. Acta* **1995,** 59, (7), 1217-1232.

59. Muller, W. E. G.; Wang, X. H.; Wiens, M.; Schlossmacher, U.; Jochum, K. P.; Schroder, H. C. *Biochim. Biophys. Acta-Gen. Subj.* **2011,** 1810, (7), 713-726.

60. Andreeva, A.; Howorth, D.; Chothia, C.; Kulesha, E.; Murzin, A. G. *Nucleic Acids Res.* **2014,** 42, (D1), D310-D314.

61. Jin, W.; Brennan, J. D. *Anal. Chim. Acta* **2002,** 461, (1), 1-36.

62. Gonzalez-Perez, A.; Persson, K. M.; Lipnizki, F. *Water* **2018,** 10, (7), 11.

63. Gonzalez-Perez, A.; Persson, K. M.; Taboada, P. *J. Mol. Liq.* **2018,** 257, 26-31.

64. Mangiatordi, G. F.; Alberga, D.; Trisciuzzi, D.; Lattanzi, G.; Nicolotti, O. *Int. J. Mol. Sci.* **2016,** 17, (7), 18.

65. Ip, Y. K.; Soh, M. M. L.; Chen, X. L.; Ong, J. L. Y.; Chng, Y. R.; Ching, B. Y.; Wong, W. P.; Lam, S. H.; Chew, S. F. *PLoS One* **2013,** 8, (4), 14.

66. Lu, M. Q.; Lee, M. D.; Smith, B. L.; Jung, J. S.; Agre, P.; Verdijk, M. A. J.; Merkx, G.; Rijs, J. P. L.; Deen, P. M. T. *Proc. Natl. Acad. Sci. U. S. A.* **1996,** 93, (20), 10908-10912.

67. Hasegawa, H.; Ma, T. H.; Skach, W.; Matthay, M. A.; Verkman, A. S. *J. Biol. Chem.* **1994,** 269, (8), 5497-5500.

68. Furman, C. S.; Gorelick-Feldman, D. A.; Davidson, K. G. V.; Yasumura, T.; Neely, J. D.; Agre, P.; Rash, J. E. *Proc. Natl. Acad. Sci. U. S. A.* **2003,** 100, (23), 13609-13614.

69. Yang, B. X.; Verkman, A. S. *J. Biol. Chem.* **1997,** 272, (26), 16140-16146.

70. Chang, E. W. Y.; Loong, A. M.; Wong, W. P.; Chew, S. F.; Wilson, J. M.; Ip, Y. K. *J. Exp. Zool. Part A* **2007,** 307A, (12), 708-723.

71. van Meer, G.; Voelker, D. R.; Feigenson, G. W. *Nat. Rev. Mol. Cell Biol.* **2008,** 9, (2), 112-124.

72. Koynova, R.; Caffrey, M. *Biochim. Biophys. Acta-Rev. Biomembr.* **1998,** 1376, (1), 91-145.

73. White, G. F.; Racher, K. I.; Lipski, A.; Hallett, F. R.; Wood, J. M. *Biochim. Biophys. Acta-Biomembr.* **2000,** 1468, (1-2), 175-186.

74. 100600 E. coli Extract Polar. https://avantilipids.com/product/100600 (2019-01-20),

75. Dowhan, W. *Annu. Rev. Biochem.* **1997,** 66, 199-232.

76. Gao, Y.; Cao, E. H.; Julius, D.; Cheng, Y. F. *Nature* **2016,** 534, (7607), 347-351.

77. Singer, S. J.; Nicolson, G. L. *Science* **1972,** 175, (4023), 720-731.

78. Chachisvilis, M.; Zhang, Y. L.; Frangos, J. A. *Proc. Natl. Acad. Sci. U. S. A.* **2006,** 103, (42), 15463-15468.

79. Gonen, T.; Cheng, Y. F.; Sliz, P.; Hiroaki, Y.; Fujiyoshi, Y.; Harrison, S. C.; Walz, T. *Nature* **2005,** 438, (7068), 633-638.

80. Tong, J. H.; Briggs, M. M.; McIntosh, T. J. *Biophys. J.* **2012,** 103, (9), 1899-1908.

81. Oberg, F.; Sjohamn, J.; Conner, M. T.; Bill, R. M.; Hedfalk, K. *Mol. Membr. Biol.* **2011,** 28, (6), 398-411.

82. Finsy, R. *Adv. Colloid Interface Sci.* **1994,** 52, 79-143.

83. Van Heeswijk, M. P. E.; Van Os, C. H. *J. Membr. Biol.* **1986,** 92, (2), 183-193.

84. Stober, W.; Fink, A.; Bohn, E. *J. Colloid Interface Sci.* **1968,** 26, (1), 62-69.

85. Soler-illia, G. J. D.; Sanchez, C.; Lebeau, B.; Patarin, J. *Chem. Rev.* **2002,** 102, (11), 4093-4138.

86. Wan, Y.; Zhao, D. Y. *Chem. Rev.* **2007,** 107, (7), 2821-2860.

87. Beck, J. S.; Vartuli, J. C.; Roth, W. J.; Leonowicz, M. E.; Kresge, C. T.; Schmitt, K. D.; Chu, C. T. W.; Olson, D. H.; Sheppard, E. W.; McCullen, S. B.; Higgins, J. B.; Schlenker, J. L. *J. Am. Chem. Soc.* **1992,** 114, (27), 10834-10843.

88. Zhao, D. Y.; Feng, J. L.; Huo, Q. S.; Melosh, N.; Fredrickson, G. H.; Chmelka, B. F.; Stucky, G. D. *Science* **1998,** 279, (5350), 548-552.

89. Brinker, C. J.; Lu, Y. F.; Sellinger, A.; Fan, H. Y. *Adv. Mater.* **1999,** 11, (7), 579-585.

90. Gustafsson, H.; Isaksson, S.; Altskar, A.; Holmberg, K. *J. Colloid Interface Sci.* **2016,** 467, 253-260.

91. Sing, K. S. W.; Everett, D. H.; Haul, R. A. W.; Moscou, L.; Pierotti, R. A.; Rouquerol, J.; Siemieniewska, T. *Pure Appl. Chem.* **1985,** 57, (4), 603-619.

92. Nandiyanto, A. B. D.; Kim, S. G.; Iskandar, F.; Okuyama, K. *Microporous Mesoporous Mat.* **2009,** 120, (3), 447-453.

93. Svergun, D. I.; Koch, M. H. J. *Rep. Prog. Phys.* **2003,** 66, (10), 1735-1782.

94. Brunauer, S.; Emmett, P. H.; Teller, E. *J. Am. Chem. Soc.* **1938,** 60, 309-319.

95. Barrett, E. P.; Joyner, L. G.; Halenda, P. P. *J. Am. Chem. Soc.* **1951,** 73, (1), 373-380.

96. Tamm, L. K.; McConnell, H. M. *Biophys. J.* **1985,** 47, (1), 105-113.

97. Brian, A. A.; McConnell, H. M. *Proc. Natl. Acad. Sci. U. S. A. - Biol. Sci.* **1984,** 81, (19), 6159-6163.

98. Salafsky, J.; Groves, J. T.; Boxer, S. G. *Biochemistry* **1996,** 35, (47), 14773-14781.

99. Graneli, A.; Rydstrom, J.; Kasemo, B.; Hook, F. *Langmuir* **2003,** 19, (3), 842-850.

100. Claesson, M.; Frost, R.; Svedhem, S.; Andersson, M. *Langmuir* **2011,** 27, (14), 8974-8982.

101. Ashley, C. E.; Carnes, E. C.; Phillips, G. K.; Padilla, D.; Durfee, P. N.; Brown, P. A.; Hanna, T. N.; Liu, J. W.; Phillips, B.; Carter, M. B.; Carroll, N. J.; Jiang, X. M.; Dunphy, D. R.; Willman, C. L.; Petsev, D. N.; Evans, D. G.; Parikh, A. N.; Chackerian, B.; Wharton, W.; Peabody, D. S.; Brinker, C. J. *Nat. Mater.* **2011,** 10, (5), 389-397.

102. Davis, R. W.; Flores, A.; Barrick, T. A.; Cox, J. M.; Brozik, S. M.; Lopez, G. P.; Brozik, J. A. *Langmuir* **2007,** 23, (7), 3864-3872.

103. Nordlund, G.; Ng, J. B. S.; Bergstrom, L.; Brzezinski, P. *ACS Nano* **2009,** 3, (9), 2639-2646.

104. Oliynyk, V.; Mille, C.; Ng, J. B. S.; von Ballmoos, C.; Corkery, R. W.; Bergstrom, L. *Phys. Chem. Chem. Phys.* **2013,** 15, (8), 2733-2740.

105. Isaksson, S.; Watkins, E. B.; Browning, K. L.; Lind, T. K.; Cardenas, M.; Hedfalk, K.; Hook, F.; Andersson, M. *Nano Letters* **2017,** 17, (1), 476-485.

106. Crane, J. M.; Verkman, A. S. *J. Cell Sci.* **2009,** 122, (6), 813-821.

107. Thompson, N. L.; Pearce, K. H.; Hsieh, H. V. *Eur. Biophys. J. Biophys. Lett.* **1993,** 22, (5), 367-378.

108. Poo, M. M.; Cone, R. A. *Nature* **1974,** 247, (5441), 438-441.

109. Liebman, P. A.; Entine, G. *Science* **1974,** 185, (4149), 457-459.

110. Bucknall, D. G.; Penfold, J.; Webster, J. R. P.; Zarbakhsh, A.; Richardson, R. M.; Rennie, A.; Higgins, J. S.; Jones, R. A. L.; Thomas, R. K.; Roser, S.; Dickinson, E. In *SURF - a second generation neutron reflectometer*, Proceedings of the meetings ICANS-XIII and ESS-PM4 Volume I, Switzerland, 1995; Paul Scherrer Institut: Switzerland, p 440.

111. Penfold, J.; Richardson, R. M.; Zarbakhsh, A.; Webster, J. R. P.; Bucknall, D. G.; Rennie, A. R.; Jones, R. A. L.; Cosgrove, T.; Thomas, R. K.; Higgins, J. S.; Fletcher, P. D. I.; Dickinson, E.; Roser, S. J.; McLure, I. A.; Hillman, A. R.; Richards, R. W.; Staples, E. J.; Burgess, A. N.; Simister, E. A.; White, J. W. *J. Chem. Soc.-Faraday Trans.* **1997,** 93, (22), 3899-3917.

112. Li, Y.; Yip, W. T. *J. Am. Chem. Soc.* **2005,** 127, (37), 12756-12757.

113. Kaehr, B.; Townson, J. L.; Kalinich, R. M.; Awad, Y. H.; Swartzentruber, B. S.; Dunphy, D. R.; Brinker, C. J. *Proc. Natl. Acad. Sci. U. S. A.* **2012,** 109, (43), 17336-17341.

114. Begu, S.; Durand, R.; Lerner, D. A.; Charnay, C.; Tourne-Peteilh, C.; Devoisselle, J. M. *Chem. Commun.* **2003**, (5), 640-641.

115. Braun, S.; Rappoport, S.; Zusman, R.; Avnir, D.; Ottolenghi, M. *Mater. Lett.* **1990,** 10, (1-2), 1-5.

116. Dave, B. C.; Dunn, B.; Valentine, J. S.; Zink, J. I. *Anal. Chem.* **1994,** 66, (22), A1120-A1127.

117. Bhatia, R. B.; Brinker, C. J.; Gupta, A. K.; Singh, A. K. *Chem. Mat.* **2000,** 12, (8), 2434-2441.

118. Kasianowicz, J. J.; Brandin, E.; Branton, D.; Deamer, D. W. *Proc. Natl. Acad. Sci. U. S. A.* **1996,** 93, (24), 13770-13773.

119. White, S. H.; Wimley, W. C. *Annu. Rev. Biophys. Biomolec. Struct.* **1999,** 28, 319-365.

120. Begu, S.; Girod, S.; Lerner, D. A.; Jardiller, N.; Tourne-Peteilh, C.; Devoisselle, J. M. *J. Mater. Chem.* **2004,** 14, (8), 1316-1320.

121. Kelly, S. M.; Price, N. C. *Curr. Protein Pept. Sci.* **2000,** 1, (4), 349-384.

122. Kelly, S. M.; Jess, T. J.; Price, N. C. *BBA-Proteins Proteomics* **2005,** 1751, (2), 119-139.

123. Plasencia, I.; Survery, S.; Ibragimova, S.; Hansen, J. S.; Kjellbom, P.; Helix-Nielsen, C.; Johanson, U.; Mouritsen, O. G. *PLoS One* **2011,** 6, (2), 9.

124. Hansen, J. S.; Vararattanavech, A.; Plasencia, I.; Greisen, P. J.; Bomholt, J.; Torres, J.; Emneus, J.; Helix-Nielsen, C. *Biochim. Biophys. Acta-Biomembr.* **2011,** 1808, (10), 2600-2607.